OVERPRINTED ALLOCYCLIC PROCESSES BY TIDAL RESONANCE IN AN EPICONTINENTAL BASIN: THE UPPER JURASSIC CURTIS FORMATION, EAST-CENTRAL UTAH, USA

VALENTIN ZUCHUAT[1], ARVE R.N. SLEVELAND[1], ROSS P. PETTIGREW[2], THOMAS J.H. DODD[2/3], STUART M. CLARKE[2], OLE RABBEL[1], ALVAR BRAATHEN[1], and IVAR MIDTKANDAL[1]

[1]Tectonostratigraphic Research Group, University of Oslo, Sem Sælands Vei 1, 0371 Oslo, Norway

[2]Basin Dynamics Research Group, Keele University, Keele, Staffordshire, ST5 5BG, United Kingdom

[3]British Geological Survey, the Lyell Centre, Research Avenue South, Edinburgh, EH14 4AP, United Kingdom

Corresponding author: valentin.zuchuat@geo.uio.no

ABSTRACT

Modern, tide-dominated and tide-influenced coastlines are characterised by a range of environments, including deltas, estuaries, and lagoons. However, some tide-dominated basins and related sedimentary units in the rock record, such as the semi-enclosed, shallow, Utah-Idaho Trough foreland basin of the Jurassic Curtis sea, do not correspond to any of these modern systems. Persistent aridity caused the characteristic severe starvation of perennial fluvial input throughout this basin, in which the informal lower, middle, and upper Curtis, as well as the underlying Entrada Sandstone, and the overlying Summerville Formation were deposited. Wave energy was efficiently dissipated by the shallow basin's elongated morphology (approximately 800x150 km), as its semi-enclosed morphology further protected the system from significant wave impact. Consequently, the semi-enclosed, shallow-marine system was dominated by amplified tidal forces, resulting in a complex distribution of heterolithic deposits.

Allocyclic forcing strongly impacted upon the system's intrinsic autocyclic processes as the lower Curtis was deposited. Short-lived relative sea-level variations, along with uplift and deformation episodes, resulted in the accumulation of three parasequences, each separated by traceable flooding and ravinement surfaces. The subsequent transgression, which defines the base of the middle Curtis, allowed for the shallow-marine part of the system to enter into tidal resonance as a consequence of the flooded basin reaching the optimal configuration of approximately 800 km in length, corresponding to an odd multiple of the quarter of the tidal wavelength given an average minimum water depth of 20

to 25 m. This resonant system overprinted the effects of allocyclic forcing and related traceable stratigraphic surfaces. However, the contemporaneous and neighbouring coastal dune field sedimentary rocks of the Moab Member of the Curtis Formation, characterised by five stacked aeolian sequences, as well as the supratidal deposits of the Summerville Formation, lingered to record allocyclic signals, as the Curtis sea regressed.

This study shows that a tide-dominated basin can enter into tidal resonance as it reaches its optimal morphological configuration, leading to the overprinting of otherwise dominant allocyclic processes by autocyclic behaviour. It is only by considering the sedimentological relationships of neighbouring and contemporaneous depositional systems that a full understanding of the dynamic stratigraphic history of a basin alternatively dominated by autocyclic and allocyclic processes can be achieved.

Keywords Aeolian sequences, allocyclic processes, autocyclic processes, Curtis Formation, stratigraphic surfaces, tidal resonance.

INTRODUCTION

Oceanic tides and their spatio-temporal variability are complex and dynamic phenomena (Kvale, 2012). The environments they act upon have raised people's interest as early as first century AD, when Pliny the Elder described areas "invaded twice each day and night by the overflowing waves of the ocean", leaving wonder if they "are to be looked upon as belonging to the land, or whether as forming portion of the sea?" (translation from Bostock & Riley, 1855).

Sedimentary successions deposited within tide-dominated basins are characterised by a three-dimensional (3D), complex and potentially cyclic assemblage of heterolithic lithologies, the distribution of which depends on a fine balance between (i) basin configuration and the dispersal of basinal hydrodynamic forces, (ii) autogenic basin processes, such as the avulsion of tidal channels, and (iii) sediment input (Kvale, 2012; Wang, 2012, and references therein). Spatio-temporal variations of tidal currents, which variably influence the system's erosion-transport-deposition chain, further complicate the arrangement of these deposits. (Kvale, 2012; Wang, 2012; Baas *et al.*, 2016). These intrinsic and interacting processes, and their associated patterns of sedimentation, are ultimately governed by

allocyclicly driven phenomena (Osleger, 1991), such as variations in relative sea-level and changes in available accommodation, and by the rate and frequency at which they occur (Strasser *et al.*, 1999). To complicate further the interpretation of the deposits of a tide-dominated basin, sediment deposition typically takes place upon a low-gradient slope and facies belts are shifted over large horizontal distances by comparatively small variations in water depth (Midtkandal & Nystuen, 2009; Zuchuat *et al.*, 2018). In addition, modern-day, semi-enclosed basins, such as the Gulf of California, the Adriatic Sea, the Persian Gulf, or the Bay of Fundy, demonstrate that basin geometry can further amplify tidal forces, allowing the system to enter a tidal resonant stage if the length of the basin approximates to an odd multiple of a quarter of the tidal wavelength (Sztanó & de Boer, 1995; Martinius & Gowland, 2011; Roos & Schuttelaars, 2011; Longhitano *et al.*, 2012; Reynaud & Dalrymple, 2012; Shaw *et al.*, 2014). A consequence of this is augmented tidal ranges and stronger tidal currents closer to the shoreline than in open water (Godin, 1993; Sztanó & de Boer's, 1995; Yoshida *et al.*, 2007; Martinius & Gowland, 2011; Roos & Schuttelaars, 2011; Longhitano *et al.*, 2012; Reynaud & Dalrymple, 2012; Shaw *et al.*, 2014).

The impact of such autocyclic processes has been detected in sediments deposited in transgressive settings, as the system's resonance typically increases with a relative sea-level rise (Sztanó & de Boer's, 1995; Martinius & Gowland, 2011; Longhitano *et al.*, 2012; Reynaud & Dalrymple, 2012; references therein). However, the time required to trigger or abandon a tidal resonance is geologically instantaneous, and the time interval encapsulated by the deposited sediments can be short, compound, and spatially variable, as different parts of the basin become resonant at different times (Reynaud & Dalrymple, 2012).

Despite a complicated and spatio-temporally compartmentalised sedimentary architecture, tidally dominated sedimentary successions typically host reservoir grade sandstone bodies that are often laterally and vertically sealed by finer grained, low porosity and low permeability sediments. Consequently, these sedimentary systems have significant potential in containing reservoir targets for the hydrocarbon exploration industry, aquifer appraisal, and CO_2 sequestration projects (Martinius *et al.*, 2005; Halland *et al.*, 2014).

Notwithstanding the inherent complexities of sediment character and distribution, most shallow-water, tide-dominated, coastal depositional systems can be classified as (i) transgressive, upward-fining estuaries, (ii) (semi-) protected lagoons, (iii) prograding, tide-dominated deltas, or (iv) open-coast tidal

flat (Fig. 1; Boyd *et al.*, 1992; Dalrymple *et al.*, 1992; Harris *et al.*, 2002; Fan, 2012). However, not every sedimentary succession that displays evidence of tidal reworking corresponds to one of these four end members. Broad, shallow epicontinental basins (Tape *et al.*, 2003; Zuchuat *et al.*, 2018), and fluvially starved macro-embayments (Zuchuat *et al.*, 2018) may display strong evidence for tidal reworking of sediments within them, but a lack of modern day equivalents hampers interpretation of the sedimentary record, especially when 3D continuous exposure is unavailable.

The continuous and three dimensional exposure of the middle to upper Jurassic succession of east-central Utah (Fig. 2) allows detailed investigations of a shallow-marine to marginal aeolian environment that evolves into a semi-enclosed, fluvially starved and tidally influenced, epeiric setting through time.

This study provides a detailed analysis of the Middle Jurassic Entrada Sandstone and the Upper Jurassic Curtis and Summerville formations (Wilcox & Currie, 2008) within the context of Zuchuat *et al.*'s (2018) lower, middle, and upper Curtis lithostratigraphic framework, and develops that framework further to reconstruct the kinematic history of the transition from an aeolian to a shallow-marine basin. The assessment of the Moab Member of the Curtis Formation (Caputo & Pryor, 1991; Peterson, 1994; Doelling, 2001; Zuchuat *et al.*, 2018) offers further insights into the behaviour of neighbouring aeolian deposits and their relationships to the contemporaneous shallow-marine and paralic realm. The work presented in this article identifies key sequence stratigraphic surfaces, such as flooding surfaces, that are the result of high-frequency systemic responses to varying climate conditions and changes in relative sea-level (Boulila *et al.*, 2010, 2011; Alberti *et al.*, 2012; Strasser *et al.*, 2012; Pellenard *et al.*, 2014), as well as basinal reconfiguration during the Oxfordian Age. Identified and traceable stratigraphic surfaces are probably a consequence of allocyclic forcing, but evidence for this within part of the succession is overprinted periodically by the sedimentary response to autocyclic processes, most notably when the tide-dominated embayment enters a resonant stage. Consequently, the study illustrates the value in identifying key sequence stratigraphic surfaces for correlating highly heterolithic, tidally influenced sedimentary packages.

Through an assessment of the sedimentology, and correlation of the stratigraphic relationships between the Entrada Sandstone, the Curtis Formation and the Summerville Formation in the vicinity of the San Rafael Swell area of south-central Utah (Fig. 2), this study has the following aims: i) to demonstrate that dominant allocyclic signatures in the sediments can be overprinted and obliterated

by those of autogenic processes, and ii) to understand and interpret shallow-marine systems, in settings where overprint occurs, through a knowledge of neighbouring and contemporaneous systems in order to fully assess the basin's history.

GEOLOGICAL SETTING

Tectonic setting

Four major tectonic events have impacted on Utah's geological development since the early Mesozoic, and the rise of the North American Cordillera (Hintze & Kowallis, 2009; Thorman, 2011; Anderson, 2015; Yonkee & Weil, 2015; and references therein): (i) the Nevadan Orogeny (Middle Jurassic-Lower Cretaceous), whose granitic intrusions can be observed at today's Utah-Nevada border, (ii) the Elko Orogeny (Middle Jurassic), characterised by alternating episodes of tectonic contraction and extension, accompanied by the development of SSW-NNE-striking, stacked foreland basin development, (iii) the Sevier Orogeny (Lower Cretaceous to Palaeogene), featuring thin and thick-skinned, east-directed fold-thrust belt structures in Idaho-Utah-Wyoming , and (iv) the Laramide Orogeny (Upper Cretaceous to Palaeogene), associated with the development of basement-rooted monoclines, such as the San Rafael Swell (Bump & Davis, 2003). The stratigraphy of central-eastern Utah was also affected by diapirism and remobilisation of the Paradox Basin evaporitic strata (Trurgill, 2011), as well as by the Colorado Plateau uplift and its sub-regional to regional extensional episodes (Levander *et al.*, 2011; Murray *et al*., 2016). The igneous intrusive complexes of the Abajo, Henry, and La Sal Mountains (Upper Oligocene) also impacted on the sedimentary strata in central-eastern Utah (Sullivan *et al*., 1991; Nelson, 1997). The Upper Callovian to Lower Oxfordian Entrada-Curtis-Summerville lithostratigraphic sub-divisions were deposited within the Utah-Idaho Trough, a SSW-NNE-oriented retroarc foreland basin at the foot of the Elko Highlands (Thorman, 2011), which the northerly-located Sundance Sea flooded several times during its history (Hintze & Kowallis, 2009).

Stratigraphy

The Middle Jurassic coastal to shallow-marine Temple Cap Formation, the shallow to marginal-marine Carmel Formation, the continental Entrada Sandstone of south-eastern Utah, and the overlying Upper Jurassic Curtis and Summerville formations comprise the San Rafael Group of the Colorado Plateau (Fig. 2; Gilluly & Reeside, 1928; Pipiringos & O'Sullivan, 1978; Peterson & Pipiringos, 1979; Anderson

147 & Lucas, 1994; Doelling, 2001; Sprinkel *et al.*, 2011a; 2011b; Doelling *et al.*, 2013). These
148 successions represent five upward-thinning, transgressive-regressive (TR) sequences with an
149 eastward and southward-wedging geometry that is a consequence of deposition within the Utah-Idaho
150 Trough (Fig. 2B; Anderson & Lucas, 1994; Brenner & Peterson, 1994; Peterson, 1994; Bjerrum &
151 Dorsey, 1995; Thormann, 2011).

152 As the Jurassic shallow and epeiric Sundance Sea regressed northward during the Callovian Age and
153 warm arid conditions prevailed, sediments of the shallow to marginal-marine Carmel Formation (Fig.
154 2C) were overlain conformably by those of the marginal-marine to continental, rusty-red to light-
155 orange, aeolian Entrada Sandstone (Fig. 2C; Gilluly & Reeside, 1928; Peterson, 1994; Hintze &
156 Kowallis, 2009). Recent $^{40}Ar/^{39}Ar$ age determinations of tephra layers within the uppermost strata of
157 the Entrada Sandstone in southern Utah provide an Oxfordian depositional date of 160.8 ± 0.4 Ma
158 (Dosset, 2014). In east-central Utah, the Entrada Sandstone is divided typically into (i) the Slick Rock
159 Member that comprises aeolian dune and interdune sediments, and (ii) the overlying and partially
160 contemporary informal unit of the 'earthy facies' (Imlay, 1952), characterised by repeated, yet
161 extraneously vegetated, mottled loess strata, interbedded with marginal-marine sabkha-like deposits
162 (Witkind, 1988; Doelling *et al.*, 2015; and references therein). The Entrada Sandstone thickens
163 westwards, in the direction of the Utah-Idaho Trough, and northwards, toward the Uinta Mountains
164 (Fig. 2; Witkind, 1988; Crabaugh & Kocurek, 1993; Kocurek & Havholm, 1993; Carr-Crabaugh &
165 Kocurek, 1998; Mountney, 2012; Doelling *et al.*, 2015). The earthy facies thins out to the south and
166 east of the study area (Fig 2B), where the sediments of the Curtis Formation directly overlie the Slick
167 Rock Member. Recycled fluvial sediments are the main constituents of the Entrada Sandstone,
168 indicative of a drainage system that originated from basement rocks of today's Appalachian Mountains
169 (Dickinson & Gehrels, 2009, 2010). Four 'construction-destruction' sequences (*sensu* Mountney,
170 2006), related to regional base-level oscillations, are recognised within this coastal aeolian system
171 (Carr-Crabaugh & Kocurek, 1998; Kocurek & Lancaster, 1999; Kocurek, 2003; Mountney, 2012), and
172 the Entrada Sandstone is capped at its top by the regional, polygenetic, and heterochronous J-3
173 Unconformity (Zuchuat *et al.*, 2018, in press), first defined by Pipiringos and O'Sullivan (1978). The
174 unconformity displays relief with an amplitude ranging from 0.1 m to 23 m, and a wavelength varying
175 from the decimetre to the hectometre scale (Zuchuat *et al.*, in press). Relief was generated by both
176 erosion-related and deformational processes, and surface types include flat angular unconformities,

177 paraconformities, steep tidal incisions, sinuous undulations, irregular tidal ravinement surfaces,
178 circular collapse structures, sedimentary loading, and hydroplastic sagging (Zuchuat *et al.*, in press).

179 The Entrada Sandstone is overlain by the lower Oxfordian Curtis Formation, originally defined by
180 Gilluly and Reeside (1928) from exposures along the northeast margin of the San Rafael Swell (Fig.
181 2). The Curtis sediments comprise complexly-arranged, shallow-marine packages of tidally influenced
182 heterolithic strata (Kreisa & Moiola, 1986; Caputo & Pryor, 1991; Wilcox & Currie, 2008; Ogg *et al.*,
183 2016; Zuchuat *et al.*, 2018) deposited as the Curtis sea flooded a gently dipping, shallow, and fluvially
184 starved, epicontinental basin that developed as the rate of accommodation development diminished at
185 end of the Callovian Age (Thorman, 2011; Zuchuat *et al.*, 2018). The underrepresentation of wave-
186 related structures within the Curtis Formation can be attributed to the protected nature of the Curtis
187 sea, as well as the elongate basin configuration, which facilitated dissipation of wave energy (Yoshida
188 *et al.*, 2007). Sediments of the Curtis Formation have a green to white colouration, which is due to the
189 presence of glauconite and chlorite. The colour strongly contrasts with the underlying rusty-red
190 terrestrial Entrada Sandstone (Gilluly & Reeside, 1928; Caputo & Pryor, 1991; Peterson, 1994).

191 It is possible to infer the Curtis sea basin reached approximately 800 km in length (Peterson, 1994;
192 Dickinson & Gehrels, 2003), and at least 150 km in width, based on stratigraphic relationships
193 between the studied Curtis-Summerville interval, and equivalent succession in neighbouring areas: the
194 Curtis-Summerville interval is the lateral equivalent of the Stump Formation further north in the Uinta
195 Mountains area (Fig. 2A; Pipiringos & Imlay, 1979; Imlay, 1980; Wilcox & Currie, 2008). It corresponds
196 to the Redwater Shale Member of the Sundance Formation in Wyoming (Imlay, 1947, 1980); and to
197 the Stump Formation in the vicinity of the Wyoming-Idaho border (Mansfield & Roundy, 1916;
198 Pipiringos & Imlay, 1979; Imlay, 1980). As a result, the Curtis Formation is characterised by an east
199 and south-wedging geometry, with a maximum thickness of approximately 80 m at Sven's Gulch (9*),
200 in the San Rafael Swell area (Gilluly & Reeside, 1928; Caputo & Pryor, 1991; Peterson, 1994;
201 Thorman, 2011; Anderson, 2015; see fig. 2 and fig. 3 in Zuchuat *et al.*, 2018). The Curtis Formation is
202 separated into three informal units based upon their outcrop character: the lower, middle, and upper
203 Curtis (Fig. 2; Zuchuat *et al.*, 2018). The lower Curtis comprises laterally restricted upper shoreface to
204 beach deposits, grading into thinly bedded, dark-green to grey, heterolithic subtidal flat deposits in
205 which gravel-rich, subtidal channels and dunes occur (Zuchuat *et al.*, 2018). The overlying middle

* Numbers in parenthesis following the names of places refer to locality numbers on Fig. 2.

Curtis is characterised by a lighter coloured and better sorted sandstone by comparison to the underlying heterolithic lower Curtis (Zuchuat *et al.*, 2018). Its base corresponds to the regional Major Transgressive Surface (MTS), and consists of complex arrangements of subtidal channels, subtidal to intertidal dune and flat deposits (Zuchuat *et al.*, 2018). The dark green, upper Curtis conformably overlies the middle Curtis, and comprises thinly bedded, subtidal to intertidal deposits, which grade into the supratidal deposits of the Summerville Formation (Zuchuat *et al.*, 2018). Towards the Utah-Colorado border (Fig. 2), these deposits form lateral and contemporaneous equivalents to the aeolian deposits that form the Moab Member of the Curtis Formation (Caputo & Pryor, 1991; Peterson, 1994; Doelling, 2001; Zuchuat *et al.*, 2018).

In the study area (Fig. 2), the Upper Curtis is overlain conformably by dark brown, sabkha deposits of the Summerville Formation (Gilluly & Reeside, 1928; Caputo & Pryor, 1991; Peterson, 1994; Lucas, 2014). However, in what were unflooded neighbouring regions to the east and to the south, the Summerville Formation likely formed as a contemporaneous coastal plain environment (Zuchuat *et al.*, 2018).

In the 'Four Corners' area, where the states of Utah, Colorado, Arizona and New Mexico meet (Fig. 2A), the Todilto Member of the Wanakah Formation is the lateral equivalent of the Curtis Formation, whereas the Beclabito Member of the Wanakah Formation corresponds to the Summerville Formation (Fig. 2C; Condon & Huffman, 1988, Kocurek *et al.*, 2018; Zuchuat *et al.*, 2018,).

The Curtis-Summerville interval corresponds to Peterson's (1994) fifth (TR) cycle within the Jurassic system of the Sundance Sea and the Western Interior Basin (Pipiringos & O'Sullivan, 1978; McMullen *et al.*, 2014), and likely corresponds to the LZA-2.3 third-order TR-interval of Haq *et al*. (1987), post calibration onto Wilcox and Currie's (2008) age and Ogg and others' (2016) timescale.

DATA AND METHODS

The data necessary for this study were gathered during three field campaigns between 2015 and 2018. The study area in central-eastern Utah (Fig. 2) extends from the Humbug Flats (1 to 5), north of the San Rafael Swell, southward to Notom Ranch (35), 44 km southwest of Hanksville, and from Last Chance Desert (38 and 39) on the western margin of the San Rafael Swell, eastward to Big Pinto Mesa (30) on the Utah-Colorado border. In order to cover the study area systematically along the exposure of the Entrada-Curtis-Summerville interval, 43 localities were visited (Fig. 2). Of these, 41

outcrop sections were measured and a total of 2291 m were logged across the Entrada-Curtis-Summerville stratigraphic interval. A total of 869 palaeocurrent readings were collected from 3D exposed dunes and ripples. Additional structural information was collected, including the dip and dip direction of sedimentary strata, fractures and faults, as well as the magnitude of fault displacements. Standard techniques in lithofacies analysis and architectural-element analysis (Walker, 1992) were used in order to permit interpretation of depositional settings. To augment the sedimentary detail, 35 m of section covering the Entrada-Curtis-Summerville interval were logged using a hand-held gamma-ray spectrometer in full assay mode at 20 cm intervals. The gamma-ray data allowed for the extraction of thorium and uranium values, which were used to determine the degree of continental involvement or the marine influences over the paralic deposits (Fertl *et al.,* 1982). Interpretation of these data must be considered within the context of the sediment calibre: thorium/uranium (Th/U) ratios as a discriminator of marine over continental provenance are reliable in mud-dominated successions (Fertl *et al.,* 1982), yet they remain relevant for coarser-grained sediments as well (Svendsen & Hartley, 2001).

This dataset is complemented by aerial images, photographic material collected at and between the visited localities using standard, handheld cameras, and unmanned aerial vehicles (UAV). In order to document, illustrate and understand the complex 3D sedimentary architecture of the interval of interest, 3D virtual outcrop models were produced from the collected photogrammetric material (after Westoby *et al.*, 2012). The models were generated using PhotoScan Pro© (Agisoft LLC, St. Petersburg, Russia), before being analysed and interpreted with Lime©, a software developed by the Virtual Outcrop Geology (VOG) group of both Bergen and Aberdeen universities (Bonaventura *et al.*, 2017; Buckley *et al.*, 2017).

Merging sedimentary data with photogrammetric models and structural data sets provided a means of tracing key sequence stratigraphic surfaces, such as subaerial unconformities, transgressive surfaces, regressive surfaces of marine erosion, flooding surfaces, and tidal ravinement surfaces (*sensu* Catuneanu, 2006; Catuneanu *et al*., 2009) to provide a regional sequence stratigraphic framework and interpretation.

RESULTS

The facies (Table 1) and facies associations (FA) schemes (Table 2) which are developed in this work summarise Zuchuat *et al.*'s (2018) detailed sedimentological assessment of the Curtis Formation and its neighbouring units. Combined with an understanding of the J-3 Unconformity development (described by Zuchuat *et al.*, in press), they are used to decipher the dynamic history of the basin, and to identify depositional environments and their spatiotemporal relationships.

Facies Association 1 – Coastal Wet Aeolian Deposits

Description: The Entrada Sandstone at the base of the studied interval comprises two facies associations that are broadly comparable to the unit's lithostratigraphic subdivisions. FA 1a consists of mostly cross-stratified aeolian dunes and interdune deposits belonging to the Slick Rock Member of the Entrada Sandstone. FA 1b corresponds to the rusty-red, informal earthy facies of the Entrada Sandstone, and comprises parallel-laminated to mottled siltstone and very fine-grained sandstone, with interdigitating trough cross-stratified sandstone, rippled cross-stratified sandstone, evaporitic beds, and isolated dunes (Figs 3A, B and 4, Table 2). FA 1b thickens north-westwards, and pinches out southwards around Notom Ranch (35), and eastwards in the vicinity of Moab (Fig. 2). Processed gamma-ray data from Duma Point (19) (Fig. 5) provide thorium/uranium ratios of approximately 5.

FA 1 is capped by the polygenetic, heterochronous, and diachronous (Zuchuat *et al.*, in press) J-3 Unconformity of Pipiringos and O'Sullivan (1978). Locally, erosive scours at the top of the FA 1b are infilled with matrix-supported, chaotically arranged conglomerates, comprising rounded to well-rounded extra-basinal pebbles and cobbles (Fig. 6A, B and C).

Interpretation: FA 1a corresponds to a coastal wet aeolian dune system (after Mountney, 2012), whereas the contemporaneous FA 1b strata were deposited within a marginal-marine, sabkha-like environment at the fringe of the Slick Rock Member palaeo-erg, where isolated coastal aeolian dunes migrated and loess were intermittently deposited. The erosive scours at the top of the unit are interpreted as the product of flash floods predating the transgression of the Curtis sea, and the accompanied deposits settled as the flows decelerated. Except for these flash flood deposits and some episodic fluvial terminal splays (Valenza, 2016), evidence for major fluvial development is

lacking within the Entrada Sandstone. The thorium/uranium ratios of 5 suggest a more prominent marine origin for these sediments, rather than a fully continental provenance (Fertl *et al.,* 1982).

Facies Association 2 – Beach to Upper Shoreface Deposits

Description: In the northern and western parts of the study area, notably at Sven's Gulch (9), Interstate 70 (12) and Shadscale Mesa (13), the surface of the J-3 Unconformity was locally modified as an approximately 2 m thick, laterally restricted (200-500 m) fine-grained sandstone (FA 2; Figs 3C and 4, Table 2), locally deforming its substratum by loading. The lowermost sandstones are plane parallel-stratified and planar to low-angle cross-stratified, which are overlain by trough cross-stratified sandstone and/or ripple-laminated sandstone. Mud drapes and rip-up clasts are documented at Interstate 70 (12) and Uneva Mine Canyon (14). FA 2 overlies FA 1, from which it is separated by the J-3 unconformity, which can locally display loading structures (Fig. 5).

Interpretation: FA 2 represents tidally-influenced upper shoreface deposits. These upper shoreface deposits represent the oldest deposits of the Curtis Formation (Zuchuat *et al.*, 2018).

Facies Association 3 – Subtidal Heterolithic Flat

Description: Sediments of FA 3 overlay FA 2 (or the J-3 unconformity where FA 2 is not present) and are dominated by thinly bedded and laterally extensive, heterolithic subtidal deposits, with a varying sand-to-mud ratio, ranging from mud-dominated (FA 3a), commonly observed in the northern, more distal part of the system, to sand-dominated (FA 3b), prevailing in the more proximal and southern part of the shallow-marine basin (Figs 3D and 4; Table 2). FA 3 is characterised by abundant, bi-directional ripple cross-laminated, cross-stratified, lenticular to flaser-bedded siltstone and sandstone strata (Fig. 7A, B and C). A bed typically reaches thicknesses of 3-10 cm. The base of FA 3a can be gradational, or it corresponds to a sharp and sometimes erosive surface. The base of FA 3b is either conformable, as visible in the more distal and deeper part of the system in the north (Fig. 4) where up to three stacked successions gradually transition and coarsen upward from FA 3a to FA3b. It can also correspond to a regressive surface of marine erosion in the proximal part of the study area, capable of cutting 45 m wide and 10 m deep incisions into its substrata (Fig. 3E). Despite their intraformational erosive character, deposits of FA 3a and FA 3b are often preserved passively onlapping the J-3

316 Unconformity, as they don't erode into the underlying strata of the Entrada Sandstone (Zuchuat *et al.*,
317 in press).

318 In the north of the study area, cross-stratified, heterolithic, bedforms, with concave up, erosive bases
319 and flat upper surfaces (Fig. 6A and D) form part of FA3. The infills comprise rounded to well-rounded,
320 gravel-size, extra-basinal clasts within a matrix of fine to very coarse-grained sand, with green mud
321 drapes locally observed between the gravelly foresets (Fig. 7D). Heterolithic gravelly dunes arranged
322 in thin-thick-thin cyclical bundles, with centimetre-thick mud drapes between foresets (Fig. 6A and E)
323 are also present. These deposits are characterised by a sharp but non-erosive flat base, and concave
324 down top surface, migrating on FA 3 substrata.

325 *Interpretation*: FA 3 heterolithic deposits testify of oscillating energy within the system (Kvale, 2012).
326 The three upward-coarsening trends observed notably in the northern part of the study area (Fig. 4)
327 indicate an increasing energy level within a gradually shallowing subtidal flat environment. Each of the
328 three upward shallowing packages are bounded by flooding surfaces, and are interpreted as
329 parasequences, *sensu* Catuneau *et al.* (2009). In the more proximal part of the shallow-marine
330 system, the erosive surfaces, sometimes observed at the base of the FA 3b, correspond to regressive
331 surfaces of marine erosion (RSME; Fig. 4). These RSMEs result from the basinward migration of
332 subtidal environments characterised by higher energy conditions accompanying the development of
333 the above mentioned parasequences. The occurrence of RSME's in the more proximal part of the
334 system, contrasting with their notable absence in the deeper and more distal part of the basin, denotes
335 a basinward-increasing slope gradient. The bedforms, with concave up, erosive bases and flat upper
336 surfaces (Fig. 6A and D) are interpreted as subtidal channels. Their restricted occurrence in the more
337 distal and basinward part of the system, interbedded between mud-dominated heterolithic deposits of
338 FA 3a (Fig. 4), highlights the separation of the flow in the system. This is in contrast to the
339 unseparated and relatively higher energy conditions observed in the more proximal parts of the basin
340 to the south, which otherwise lead to the deposition of better sorted sediments (FA 3b)

341 *Facies Association 4 – Sand-Rich Subtidal to Supratidal Flat and Correlative Tidal Channel*
342 *Infill*

343 *Description*: FA 4 is subdivided into FA 4a and FA 4b. FA 4a comprises light-pink, very fine to fine-
344 grained sandstones that extend over tens of kilometres on the eastern margin of the San Rafael Swell,

in the southern and more proximal part of the study area (Figs 2 and 3F). FA 4a is characterised by a southward thickening (from 4 to 15 m thick) of plane parallel-bedded to plane parallel-laminated strata, with single and double mud drapes, along with rare, unidirectional current ripples and herringbone cross-stratification.

Fa 4b is restricted to the north-eastern margin of the San Rafael Swell, where it consists of a 1 to 10 m thick, multi-storey, coarse-grained, cross-stratified sandstone with rounded to well rounded, gravel size extra-basinal clasts (Fig 3G). It displays common mud drapes along foresets, reactivation surfaces, as well as bidirectional current indicators, such as subordinate-flow ripples climbing on the reactivation surfaces, and herringbone cross-stratification.

Interpretation: FA 4a and FA 4b represent a proximal subtidal to supratidal sandflat, and the correlative, more distal, gravel-rich, subtidal channels, respectively (Table 2). FA 4 occurs only within the uppermost parasequence of the lower Curtis (Parasequence 3). The grainsize and the colour of FA 4a are potentially related to the reworking of fringing deposits of the contemporaneous and neighbouring aeolian dune fields of the Slick Rock Member. FA 4 is interpreted to reflect the most prominent basinward shoreline progradation recorded by the lower Curtis, constituted by FA 2, FA 3, and FA 4. The lowermost parasequence, occurs only at Sven's Gulch (9), Cedar Mountain (43), and Sid and Charley (41) (Fig. 3D). It is characterised by steep tidal incisions (Fig. 3E). Despite evidence of current reversals within the sediments (Fig. 7A and C), the lower Curtis is dominated by a basinward (northward) current direction (Fig. 4B).

Facies Association 5 – Subtidal to Intertidal Channel-Dune-Flat Complex Description

Description: The lower Curtis is overlain disconformably by FA 5 (Figs 3H and 4A, Table 2) which represents the informal middle Curtis unit (Zuchuat *et al.*, 2018). Its base is sharp, and it can be erosive. It can be traced throughout the study area, all the way to Ghost Ranch, northern New Mexico, where it marks the base of the Todilto Member of the Wanakah Formation (Fig. 2; Zuchuat *et al.*, 2018; Zuchuat *et al.*, in press). The thickness of FA 5 varies from more than 45 m in the northern part of the study area, to approximately 1 m, as it thins south and eastwards. These sediments comprise light green to white, very fine to fine-grained well-sorted sandstone (Fig. 7E through I). Grain size fines slightly south and eastwards, where FA 5 is dominated by very fine to fine-grained sandstone. FA 5 features lenticular to wavy to flaser-bedded sandstones, with occasional laminated mudstones. It also

374 comprises climbing ripples, and intervals dominated by bidirectional herringbone cross-stratification.
375 Interference ripples occur sporadically within the succession, arranged in a near orthogonal pattern.
376 3D cross-stratified packages are observed within FA 5, with frequent reactivation surfaces and
377 counter-ripples. The cross-stratified and wavy to flaser-bedded sandstone strata are locally arranged
378 in centimetre to metre-scale tidal bundles with varying amounts of organic/argillaceous matter, often
379 deposited as single or double mud drapes. FA 5 also comprises plane parallel-stratified, and low-angle
380 cross-stratified intervals. These facies laterally interdigitate with one another over distances of 5 to 40
381 m. Individual bedforms in FA 5 reach a maximum height of 2 to 3 m, and the average bedform size is
382 one to two orders of magnitude higher than in the underlying lower Curtis deposits. Bedform thickness
383 decreases up-section, as well as south and eastwards, as FA 5 thins in these directions.
384 Palaeocurrent measurements indicate a strong bi-modal distribution of current motion at the time of
385 deposition, oriented NW-SE (Fig. 4B).

386 *Interpretation*: FA 5 corresponds to the informal middle Curtis unit (Zuchuat *et al.*, 2018). Its basal
387 surface corresponds to the MTS (Zuchuat *et al.*, 2018), which is a composite surface transgressive-
388 ravinement surface. FA 5 is interpreted as an intricate amalgamation of subtidal to intertidal channels
389 and associated tangential to sigmoidal cross-stratified sandstones arranged in tidal bundles. This
390 indicates strong cyclical tidal influence on the system with a dominant bidirectional current component.
391 Subtidal channels eroded into sandflats and subaqueous 3D dunes within a subtidal to intertidal
392 system. FA 5 reflects an overall higher energy level, evidenced by coarser-grained and better-sorted
393 sediments than compared with the underlying lower Curtis strata. The amalgamated bedforms and
394 bedform sets inhibits the recognition of any traceable stratigraphic surfaces, such as flooding surfaces
395 or regressive surfaces of marine erosion, accentuating the contrast with the underlying lower Curtis
396 shallow-marine system.

397 ### *Facies Association 6 – Upper Heterolithic Subtidal to Intertidal Flat*

398 *Description*: The middle Curtis FA 5 deposits are conformably overlain by FA 6, which consists of
399 green, siltstone to fine-grained, laterally extensive, isopachous sandstone beds, distinguished by
400 plane parallel stratification, unidirectional current ripple and herringbone cross-stratification. Individual
401 bed set thicknesses range from 3 to 40 cm, and beds become thinner up-section (Fig. 3I, Table 2). FA
402 6 crops out in the northern, central, and southern parts of the study area (Figs 4 and 8; Zuchuat *et al.*,

2018). Unlike the underlying sediments of FA5, FA 6 thins northwards, from a maximum thickness of approximately 28 m near Hanksville (34) to a minimum of 5 m at Sulphur Canyon (1) (Fig. 4).

Interpretation: FA 6 constitutes the informal upper Curtis, conformably overlying the middle Curtis (Zuchuat *et al.* 2018). It was deposited within subtidal to intertidal flat environments (Fig. 3I, Table 2), reflecting a lower energy environment with respect to those of the underlying FA 5.

Facies Association 7 – Coastal Dry Eolian Dune Field

Description: Towards the eastern part of the study area, FA 6 is replaced by FA 7, (Figs 3J and 8, Table 2). FA 7 reaches a maximum thickness of approximately 50 m close to the Utah-Colorado border, and pinches out between Duma Point (19) and Horse Flies Gulch (20). It is characterised, at its base, by very fine to fine-grained, structureless to ripple to trough cross-stratified sandstones, interbedded with green silty sandstones, commonly displaying soft sediment deformation structures. FA 7 is composed of five packages of fine-grained, cross-stratified dunes, reaching an individual maximum thickness of approximately 15-20 m at Lost Spring Canyon (28) on the eastern border of Arches National Park. Each package is capped by a traceable erosive surface, under which abundant rhizoliths can be observed (Zuchuat *et al.* 2018). These erosive surfaces can be overlain by very fine to fine-grained, ripple or herringbone cross-stratified sandstones with single and double mud drapes, and arranged in flaser-bedded packages. Undulating millimetre to centimetre-scale, structureless sandstone strata also occur on top of these erosive surfaces. The uppermost package is also overlain by a thin sandstone crust that is typically structureless.

Interpretation: FA 7 consists of aeolian dunes corresponding to Doelling's (2001) Moab Member of the Curtis Formation (Figs 3J and 8, Table 2). The traceable erosive truncations are supersurfaces (sensu Kocurek, 1988), implying that the Moab Member consists of five stacked aeolian sequences. Towards Duma Point (19), subtidal to intertidal deposits are commonly found overlying these supersurfaces, whereas supratidal deposits become more frequent towards the eastern and more continental part of the study area, linked with the development of local sand stromatolite structures similar to those described by Getty and Hagadorn (2009). These supratidal deposits are often associated with sparsely vegetated palaeosol horizons, as testified by the development of rhizoliths in the underlying strata.

Facies Association 8 – Supratidal Flat

Description: FA 8 consists of rusty red to dark brown, evaporite-rich mudstones and siltstone deposits that sharply overly the aeolian dunes of FA 7. The contact between FA 8 and the underlying strata of FA 6 subtidal to supratidal sediments is gradational (Fig. 3I and K Table 2). FA 8 also contains centimetre to decimetre-thick, light grey, ripple cross-stratified sandstone beds. The thickness and the frequency of these deposits diminish up-section. Similarly to FA 1b, the thorium/uranium ratios processed from the gamma-ray data collected at Duma Point (19) fall at approximately 5. Only three minor channels were observed within FA 8, reaching 30-50 m in width, and 0.5-1 m in depth.

Interpretation: FA 8 belongs to the Summerville Formation, and mainly consists of fine-grained supratidal, paralic to sabkha-like sediments that overly the shallow-marine deposits of the Curtis Formation. These were likely deposited as the Curtis sea regressed. The occurrence of light grey, marine-influenced strata testifies to the frequent and recurrent marine incursions that punctuated overall regression. The marine influence of FA 8 is supported by thorium/uranium values of approximately 5, similar to values observed in FA 1b. The fluvially starved aspect of the studied basin is further emphasised by the scarcity and the limited size of the fluvial channels observed in outcrop within this paralic system, contemporaneous to the neighbouring shallow-marine domain.

J-3 Unconformity

Description: The J-3 Unconformity, which separates the Entrada Sandstone from the Curtis Formation is characterised by eight different types of relief related to (i) erosive, or (ii) deformation-related processes. The different types of relief are classified as (a) angular unconformity, (b) paraconformity, (c) steep incisions, (d) undulating relief, (e) irregular relief, including fault-plane and erosion-related relief irregularities, (f) circular collapsed structures, (g) sedimentary loading, and (h) hydroplastic sagging (Zuchuat *et al.*, in press). The relief ranges from a centimetre-scale, to a maximum amplitude of 23 m, whereas its wavelength can reach 200 m (Zuchuat *et al.*, in press). To the east of the study area, the J-3 Unconformity merges with the MTS at the base of the middle Curtis.

Interpretation: The J-3 Unconformity composite surface, is the product of series of erosive processes, which includes aeolian deflation, superficial incision linked to flash floods, tidal ravinement during transgressive phases, and funnelling of the tidal forces as the shoreline regressed. It is important to notice that these different processes did not only impact the system in a 3D space, but they varied

with time, both in terms of intensity and location. Furthermore, each individual process and individual type of relief are non-unique, as a specific relief geometry can be produced by different processes, and one single process can generate different geometries (Burgess & Prince, 2015; Zuchuat *et al.*, in press). Therefore, the composite and highly polychronous nature of such a surface implies that it cannot be regarded as a genuine time barrier, and thus, as an unconformity *sensu stricto*.

DEPOSITIONAL MODEL

Several authors have presented the Curtis and Summerville formations as an overall transgressive-regressive cycle (Caputo & Pryor, 1991; Wilcox & Curie 2008; Peterson, 1994). This study supports their interpretation as a general conclusion, but the spatially and stratigraphically diverse body of data assembled here suggests that the detailed stratigraphic history of the interval is more intricate than that previously proposed (Fig. 9). Importantly, in low-gradient systems like the Curtis basin the interpretation of stratigraphic detail is strongly influenced by the effects of relatively minor changes in sea-level upon the position of the shoreline and, by consequence, the facies distribution (Midtkandal & Nystuen, 2009).

Pre-Curtis sea transgression

The J-3 Unconformity is intrinsically polygenetic, heterochronous, and diachronous by nature (Zuchuat *et al.* 2018; in press), comparable to the compound surface discussed by Ahokas *et al.* (2014), as the deposition of the Entrada Sandstone, the Curtis, and Summerville formations, and the accompanying relative sea-level variations, all influenced the genesis of this bounding surface. Consequently, the J-3 Unconformity is not the product of a forced regression, as suggested by Mitchum *et al.*'s (1977) definition of unconformities, but was primarily developed as the Curtis sea started to transgress from the north.

An interpretation of a composite, polygenetic, heterochronous, and diachronous J-3 Unconformity is further supported by preliminary gamma-ray data obtained from the earthy facies of the Entrada Sandstone at Duma Point (19) (Figs 5 and 8). As thorium/uranium ratios of <7 can be used to indicate marine influences within sedimentary rocks (Fertl *et al.,* 1982), recorded values in this study of approximately 5 indicate marine influences over these paralic strata. U_{excess} calculations clearly identify cyclical marine flooding (Fig. 5) in the earthy

facies of the Entrada Sandstone, but also in the supratidal deposits of the Summerville deposits. These lines of evidence together support an interpretation of the earthy facies as partly influenced by marine flooding as the early Curtis sea migrated southwards and into a coastal aeolian system in the south and eastern part of the study area (Fig. 9A and B). This was accompanied by the development of the J-3 Unconformity as a ravinement surface (Zuchuat *et al.*, in press), rather than an unconformity *sensu stricto*.

Early Curtis sea transgression

The oldest sediments of the Curtis Formation developed during the earliest flooding of the earthy facies, and correspond to FA 2 shoreface deposits. As these sedimentary bodies are constrained to certain localities (Curtis Point (7), Sven's Gulch (9), and Uneva Mine Canyon (14)), it can be regarded as evidence for pre-existing relief on the J-3 Unconformity, as palaeo-highs within the Entrada Sandstone acted as interfluves that remained unflooded until the subsequent transgression (Fig. 9B). The exact nature of these palaeo-highs remains equivocal. Nevertheless, as FA 2 typically overlies deposits of the earthy facies (FA 1b), a purely sedimentary explanation for the existence of palaeo-topography seems unlikely. They could however be linked to pre-transgression, sub-regional folding and tilting episodes (Zuchuat *et al.*, in press), which generated low-amplitude and long wavelength relief.

The transgression continued, and reached areas around Hanksville, which represents the most proximal domain of the study area (Figs 2 and 9C). As transgression progressed, the energy of the system diminished and the subtidal heterolithic successions of FA 3 were deposited. The eastern part of the study area remained unaffected by the marine flooding. Sub-regional uplift episodes, coupled with the erosive nature of the MTS that accompanied deposition of the middle Curtis (Zuchuat *et al.*, 2018, in press), mean that the western extent of the transgression remains unconstrained.

FA 3a mud-dominated deposits, which are more common in the northern parts of the study area, represent a tidally influenced distal domain of the Curtis sea, whereas the coarser grained, sand-dominated FA 3b strata are concentrated towards the more proximal domain of tidal influence in the south (Fig. 4; Zuchuat *et al.*, 2018). The proximal sediments (FA3b) are characterised by better-sorted and coarser grained deposits compared to the distal setting (FA 3a). However, occasional localities within the more distal domain of the Curtis, such as Cedar Mountain (43), sometimes can display a

succession dominated by FA 3b. Textural trends such as these, which show an increase in the degree of sorting and grain size with increasing proximity to the coastline are in direct contrast to the classical 'coarse to fine-grained', trend observed within modern-day, tide-dominated environments (Fig. 1; Boyd et al., 1992; Dalrymple et al., 1992; Harris *et al.*, 2002; Fan, 2012).

The exclusive occurrence of the gravel-rich dunes and conglomeratic subtidal channels at the localities north of Dry Mesa (6) and Last Chance Desert (38, 39) (Fig. 6), may be symptomatic of tidally influenced environments, in which higher energy tidal currents were in operation. Palaeo-current indicators from the lower Curtis (Fig. 4) and basinward orientation of dune foresets, suggest a strong basin-floor ebb-current over the area (Fig. 4B). Each of the three major upward-shallowing successions that characterise the lower Curtis reflects short-lived variations in relative sea-level (Figs 4 and 10). Traceable erosive surfaces within the upward-shallowing successions in the more proximal part of the system (Fig. 4) are interpreted as regressive surfaces of marine erosion. Each of these surfaces testify to major basinward shifts of the facies belt across the low-gradient Curtis sea basin, followed by the deposition of the most proximal and shallowest strata of each upward-shallowing succession. These regressive surfaces of marine erosion are absent from the most distal and basinward part of the system in the north (Fig. 4); a consequence of higher slope gradients in the distal areas compared with more proximal parts of the basin. These upward-shallowing successions were subsequently flooded as the relative sea-level rose, and are thus bounded by flooding/ravinement surfaces. Consequently, the three upward-shallowing successions represent parasequences (P1, P2, P3). The steep incisions (Fig. 3E) developed at the top of the lowermost parasequence (P1) are a consequence of a short-lived, decametre scale fall in relative sea-level that accompanied the development of the second parasequence (P2) (Zuchuat *et al.*, 2018; in press). The amplitudes of the relative sea-level variations increase up-section (Fig. 10) such that FA4a proximal, subtidal to supratidal sandflat deposits (Fig. 3F), and correlative FA 4b gravel-rich, subtidal channels (Fig. 3G) prograded basinwards during the uppermost parasequence (P3), as a result of the most pronounced facies belt shift recorded within the lower Curtis (Figs 4, 9D and 10). However, despite increases in the amplitudes of relative sea-level variations during Curtis times, some of the distal parts of the basin directly adjacent to Cedar Mountain (43) (Fig. 11) were less influenced by relative sea-level variations during the development of P3 than their more proximal counterparts, as FA 4b subtidal channels did not reach these distal areas.

Major Transgression

The top of the lower Curtis is capped by the MTS as a consequence of an abrupt relative sea-level rise which completely flooded the study area (Fig. 9E), and the area as far south as the present day New Mexico border (Zuchuat *et al.*, 2018; in press). This surface is a complex arrangement of paraconformities and disconformities (Zuchuat *et al.*, 2018; in press). The area between Interstate 70 (12), Shadscale Mesa (13), and Uneva Mine Canyon (14), as well as Cedar Mountain (43) (Fig. 11), shows evidence of sub-regional, early Oxfordian uplift prior to the Major Transgression in the lower Oxfordian (Zuchuat *et al.*, 2018; in press), as the MTS truncates lower Curtis strata with an angular relationship.

The sediments of FA 5, particularly subaqueous dunes with associated abundant reactivation surfaces, and sandflats with a strong bidirectional current component (Figs 6I and 7E through H) are in stark contrast to the underlying lower Curtis strata and suggest a higher energy level within the marine system by middle Curtis times (Figs 10 and 12). Grain sizes generally fine toward the coastline and the middle Curtis thickens toward the distal basin (Zuchuat *et al.*, 2018), as is common in many modern-day, tide-dominated environments (Fig. 1; Boyd *et al*., 1992; Dalrymple *et al.*, 1992; Harris *et al.*, 2002; Fan, 2012). The partial flooding of the Slick Rock Member resulted in the reworking of these aeolian dunes sediments into the deposits of the middle Curtis (Figs 4 and 8; Dickinson & Gehrels, 2009, 2010).

A distinctive characteristic of the middle Curtis is the amalgamation of cross-stratified bedforms, coupled with the absence of traceable stratigraphic surfaces (Figs 4 and 10). Such a dramatic shift in sedimentology within an elongated, semi-enclosed basin of this size may be interpreted as the onset of tidal resonance within the Curtis sea resulting in overprinting of any significant sedimentary response to allocyclic forcing by autocyclic processes (Godin, 1993; Sztanó & de Boer, 1995; Yoshida *et al.*, 2007). Because the system enters tidal resonance, and the signatures of autocyclic processes dominate the sediments, it is impossible to trace a maximum flooding surface (MFS) across localities (Figs 4 and 10). However, upward-thinning, and upward-fining of FA 5 deposits, as well as the overall up-section progradation of the sediments, suggest that a MFS is likely to be located within the lowermost few metres of the middle Curtis (Fig. 10).

Curtis sea Regression

As the Curtis sea retreated rapidly from the eastern inundated coastal plains, the system saw the concomitant development of a dry aeolian dune system (FA7; Kocurek & Havholm, 1993; Kocurek & Lancaster, 1999; Kocurek, 2003), neighboured by an extensive supratidal flat (FA 8, Fig. 10). The calm and restricted setting for FA 6 strata suggests deposition in the proximal and protected zones of the contemporaneous marine system, and FA 5 sediments with metre-scale bedforms were deposited in the distal setting to the west and north (Figs 8, 9F and 12). The asymmetrical, eastward-pinching FA 5 and FA 6 deposits, overlain by FA 8 supratidal sediments, and the growth of the aeolian dune fields of FA 7 (Moab Member; Figs 8 and 9G), suggest rapid coastline progradation, accompanied by increased sediment availability for aeolian transport. As a result, FA 7 thickens eastwards, and its five distinct aeolian packages may be interpreted as sequences (*sensu* Kocurek 1988) separated by subtidal to intertidal deposits in its western parts (Figs 8 and 10), and by correlative supratidal deposits, as well as by local development of palaeosol and rhizoliths towards the present day Utah-Colorado border (Zuchuat *et al.*, 2018). These five sequences of the Moab Member likely reflect humid-arid climate variations (Kocurek, 1988; Mountney, 2006, 2012) during which episodes of relative base-level fall promoted growth of the aeolian system, and transgressive phases partially inundated and terminated the aeolian dune field. The abrupt termination of dune fields of FA 7 (Fig. 9H) contrasts with the gradual infill of the contemporaneous marine basin by FA 6 and FA 8, suggesting that a major climate shift as an explanation for the termination of the dune fields cannot be justified. It is proposed that a final, short-lived marine transgression shut down the sediment supply to the aeolian system, preserved it in its final form, and deposited a thin interval (<1 m) of shallow-marine deposits to supratidal deposits, with localised sand stromatolite structures.

The relative influence of autocyclic and allocyclic processes upon the system

Sedimentary and Gamma-ray log data presented here indicate that the Entrada-Curtis-Summerville interval was influenced continuously by allocyclic processes, most notably by relative sea-level variations and climate changes, but also by sub-regional uplift episodes (Figs 5, 8 and 10; Zuchuat *et al.*, in press). The Gamma-ray log data (Fig. 8) display cyclical patterns within the studied interval, with no obvious periods of non-deposition or erosion documented in the sedimentology. The marine influence upon the sediments of the earthy facies, together with the ravinement diagnostic of the J-3

Unconformity (Zuchuat *et al.*, in press), suggest near-continuous sedimentation from the earthy facies of the Entrada Sandstone, through lower Curtis transgressive deposits, into the post-Major-Transgressive middle- and upper Curtis sediments, and associated strata of the Summerville Formation. Consequently, the succession would present an ideal candidate for future work that could analyse relative dominance of allocyclic or autocyclic processes upon sediment dispersal and the preserved strata.

During deposition of the lower Curtis, the system was not in tidal resonance, as the system responded to both autocyclic and allocyclic processes, as observed at Cedar Mountain (43) (Fig. 11). The heterogeneous energy distribution of the tidal system was responsive to minor changes in basin morphology, influencing the sediment dispersion and bedform development as part of a self-sustained feedback loop (*sensu* Cecil, 2003; de Boer *et al.*, 2011). Minor current reorganisation was probably responsible for local incisions and/or continuous deposition within each of the three parasequences (Fig. 10), in contrast to regionally significant and regionally traceable stratigraphic surfaces.

The Major Transgression and the resulting MTS, which defines the base of the middle Curtis, flooded locations beyond the extent of the present study area (Zuchuat *et al.*, 2018; in press), and allowed the system to enter a tidally resonant stage. Traceable stratigraphic surfaces generated by allocyclic relative sea-level variations were not preserved, as autocyclic processes dominated the marine system (Figs 6, 7 and 10). However, retreat of the Curtis sea was accompanied by the development of the extensive supra-tidal flats of the Summerville Formation (FA 8), and the coastal aeolian systems of the Moab Member of the Curtis Formation (FA 7). Contrary to the dominance of autocyclic process acting upon the deposits of the contemporaneous and resonant tide-dominated system, autocyclic processes impacting on FA 7 and FA 8 were strongly influenced and modulated by allocyclic relative sea-level variations and associated climate oscillations (Figs 8 and 10; Kocurek & Havholm, 1993; Kocurek, 2003; Mountney, 2006).

In addition to modulating the morphology, scale, and type of bedforms occurring within the supratidal and coastal aeolian systems, allocyclic processes were responsible for the rate at which these sediments accumulated and the cyclic arrangement of those sediments. This is visible in the vertical stacking of the aeolian sequences of the Moab Member, which are terminated by marine flooding in the areas close to the palaeo-coastline, whereas palaeosols and superficial vegetation commonly developed where the system remained unflooded by these short-lived marine transgressions.

DISCUSSION

The sequence stratigraphic model for the Entrada-Curtis-Summerville interval presented in the study interprets sediments of the Curtis Formation to be deposited in a shallow-marine to marginal-marine setting with variable tidal influence. The lower Curtis sediments (FA2 – FA4) represent early marine transgression of the Curtis sea in which three parasequences can be correlated by the flooding surfaces that bound them. The sedimentary signature of tidal influence is present within the shallowing upwards successions but it is subordinate to the effects of allocyclic controls upon the sedimentology. The middle Curtis sediments (FA5) represent a significantly higher energy environment impacted by tidal processes, but lack both wave-related sedimentary structures and surfaces of sequence-stratigraphic significance. This is interpreted as the overprinting of allocyclic sedimentary signatures by those of a dominant and localised tidal influence. Consequently, the Curtis sea was in a state of tidal resonance during middle Curtis times. The upper Curtis sediments (FA6 – FA8) display stratigraphically significant surfaces that represent marine regression, and the influence of tidal processes upon the sedimentology is subordinate.

It is important to note that similar bedforms to the ones observed in the Curtis Formation (Fig. 7) do occur in other depositional systems in which tidal currents act only as a modulating factor rather than a dominant control upon sedimentary character (Martinius & Gowland, 2011; Baas *et al.*, 2016; Gugliotta *et al.*, 2016). However, because of the lack of any major fluvial systems within the neighbouring and contemporaneous Entrada Sandstone and Summerville Formation, as well as the absence of wave current indicators, a hypothesis of a mixed-energy system for Curtis times is difficult to reconcile. The near-exclusively tidally influenced deposits of the Curtis Formation, coupled with a semi-enclosed, elongated basin configuration at the time, suggest the onset of tidal resonance is a reasonable hypothesis for the major energy jump accompanying the deposition of the middle Curtis (Sztanó & de Boer's, 1995; Martinius & Gowland, 2011; Roos & Schuttelaars, 2011; Longhitano *et al.*, 2012; Reynaud & Dalrymple, 2012; Shaw *et al.*, 2014).

Facies distribution, energy levels, basin geometry and tidal resonance

The sedimentology of the Curtis Formation suggests that energy levels within the Curtis sea during deposition of the lower Curtis sediments were generally lower than those present during deposition of the middle and upper Curtis sediments. However, the distal to proximal sedimentological trends

displayed within the lower Curtis are counter to those normally expected within tidally dominated systems (Boyd *et al.*, 1992; Dalrymple *et al.*, 1992; Harris *et al.*, 2002; Fan, 2012). They imply a generally consistent average energy level towards the coast at the time of deposition, compared to a spatial and temporal partitioning of energy levels distally (Fig. 12) that promote development of conglomeratic channels and dunes within a finer-grained matrix (Fig. 4A). This may be explained by a tidal reworking within a confined basin of extra-basinally sourced flash flood deposits (Zuchuat *et al.*, 2018), that may have originated from the neighbouring, uplifted Uncompahgre terraces to the east (Otto & Picard, 1976; Scott *et al.*, 2001), and/or from uplifted highlands to the west (Thorman, 2011; Anderson, 2015). Similar gravel to pebble to cobble sized conglomeratic bedforms are found in modern, tidally influenced and confined basins, such as the Bay of Fundy (Li *et al*., 2014; Shaw *et al.,* 2014; Todd *et al*., 2014), the San Francisco Bay (Barnard *et al*., 2006) or the bay of Brest (Gregoire *et al*., 2016). Alternatively, conglomeritic channels and dunes may result from the influx of a coarser sediment as short-lived regressive pulses brought material from the proximal part of the basin into distal areas, and regressive pulses are notable during the development of the uppermost parasequence P3 (Zuchuat *et al.*, 2018).

The southwards increase in energy, and the presence of sandier and more homogeneous strata within the more proximal parts of the system, may be linked also to tidal amplification as a result of an optimal basin configuration (Godin, 1993; Sztanó & de Boer, 1995; Yoshida *et al.,* 2007) that developed towards the end of lower Curtis times. This may be the pre-cursor to the onset of tidal resonance in middle Curtis times. The physical dimensions of the basin, along with the subdued nature of the pre-transgression relief by this time (Godin, 1993; Sztanó & de Boer, 1995; Yoshida *et al.*, 2007) may serve to promote resonance.

As the dimensions of the semi-enclosed, fluvially starved Curtis sea reached approximately 800 km in length, and at least 150 km in width, it is possible to determine whether an amphidromic tidal system (Sztanó & de Boer, 1995) could have developed that may provide an explanation for the sedimentology observed. The water depth (d) in tidal systems can be determined from the average bedform thickness of the tallest features observed in the succession (h) by (Allen, 1968):

$$h = 0.086(d)^{1.19} \quad (1)$$

In the Curtis sediments, bedform thickness h can reach 3 to 4 m, which gives a minimum approximation for the deepest waters of the Curtis sea in the study area of approximately 20-25 m.

The Rossby Deformation Radius (R) for a given palaeo-latitude approximately indicates the required basin width for an amphidromic system to develop (Sztanó & de Boer, 1995):

$$R = \sqrt{g * d}/f \quad (2)$$

where g is the gravitational acceleration (9.81 m/s^2), d is the water depth, and f is the Coriolis coefficient (8.3651*10^{-5} rad/s at 35° latitude (after Vallis' (2017) Coriolis coefficient equation; palaeolatitude after Hintze & Kowallis (2009)). The solution to equation (2) is approximately 167.5 km, which is close to the width of the Curtis sea. The calculations imply that an amphidromic system could have developed within the Curtis sea basin, but the location of the rotational centre of the tidal wave remains unknown and impossible to constrain.

Tidal resonance can develop within a semi-enclosed basin, such as the Gulf of California, the Adriatic Sea, the Persian Gulf, or the Bay of Fundy (Sztanó & de Boer, 1995; Martinius & Gowland, 2011; Roos & Schuttelaars, 2011; Longhitano *et al.*, 2012; Reynaud & Dalrymple, 2012; Shaw *et al.*, 2014), if the length of the embayment approaches an odd multiple of a quarter of the tidal wavelength (Godin, 1993; Sztanó & de Boer's, 1995; Yoshida *et al*, 2007):

$$L = T * \sqrt{g * d} \quad (3)$$

where L is the tidal wavelength, T is the period of the M2 tide (44'712 seconds; Roos & Schuttelaars, 2011), g is the gravitational acceleration (9.81 m/s^2), and d is the water depth. However, such resonant behaviour depends also upon the basal shear stresses and the subaqueous morphology of the tidal system (Roos & Schuttelaars, 2011; Wang *et al.*, 2014).

For water depths d of approximately 20 m and 25 m (equation 1), the tidal wavelength L approaches approximately 625 km, or 700 km respectively, which gives a quarter wavelength of approximately 156 km or 175 km, respectively. As these values are approximately one fifth of the total length of the Curtis sea, tidal resonance could have developed within the basin and may provide some explanation for the variation in sedimentology observed throughout Curtis times.

The phenomenon of resonance may have been triggered by the Major Transgression at the base of the middle Curtis, the regional extent and abrupt nature of which may be linked to an allocyclic, orbitally-forced, relative sea-level rise during the Lower Oxfordian (Boulila *et al.*, 2010, 2011; Strasser *et al.*, 2012; Pellenard *et al.*, 2014). The resultant tidally resonant system, as the middle and upper Curtis were being deposited, was dominated by autocyclic interactions, which overprinted the

722 stratigraphic signatures of most Lower Oxfordian, allocyclic relative sea-level variations (Boulila *et al.*,
723 2010, 2011; Strasser *et al.*, 2012; Pellenard *et al.*, 2014).

724 *Causes of cyclcity*

725 Both 405 and 100 kyr, orbitally forced eccentricity cycles have been documented within the Tethyan
726 Ocean during the Callovian and Oxfordian ages, within which $\delta^{18}O$ isotopic data indicate a cooling
727 event during the Upper Callovian Age (Boulila *et al.*, 2010, 2011; Strasser *et al.*, 2012; Pellenard *et al.*,
728 2014). Such a cooling episode, accompanied by increased sediment available for wind transport, may
729 explain the growth and demise of the Entrada aeolian system. Consequently, it may be suggested that
730 sedimentary cycles recorded in the Entrada Sandstone, the lower Curtis, the Moab Member of the
731 Curtis Formation, and the Summerville Formation (Figs 8 and 10), may be related to one (or both) of
732 these two Milankovitch-type cycles. However, the exact nature of relative sea-level variations remains
733 uncertain, and precise dating of the shallow-marine, supratidal, and aeolian deposits of the studied
734 area and their local equivalents would be required in order to determine cycle period (or frequency).
735 Considering the five aeolian sequences of the Moab Member of the Curtis Formation, each truncated
736 by shallow-marine or superficially vegetated palaeosol horizons, it seems that relative base-level/sea-
737 level oscillations and the arid-humid climate variations were responding simultaneously to the above-
738 mentioned eccentricity cycles.

739 However, short-lived episodes of sub-regional tectonic uplift have accompanied deposition of parts of
740 the Entrada-lower Curtis interval, which may have impacted upon relative sea-level within the basin
741 (Figs 10 and 11; Zuchuat *et al.*, 2018, in press). It seems unlikely that such localised uplift episodes
742 and associated relative sea-level oscillations triggered a simultaneous climate adjustment in the
743 continental, contemporaneous counterparts to the shallow-marine system. Nevertheless, multiple
744 short-lived episodes of tectonic uplift occurred during the deposition of the lower Curtis; the potential
745 climate response of the arid paralic and continental realms to such sub-regional uplift events is difficult
746 to fully assess. Furthermore, debate persists over whether the eccentricity cycles lead to small-scale,
747 glacio-eustatic sea-level variations (Dromart *et al.*, 2003; Wierzbowski *et al.*, 2009; Donnadieu *et al.*,
748 2011; Alberti *et al.*, 2012; Chumakov *et al.*, 2014), or whether these sea-level variations are due to
749 orbitally-forced cycles, of thermal water expansion and/or ground-water recharge (Schulz & Schäfer-
750 Neth, 1997; Boulila *et al.*, 2011).

The amplitude of the relative sea-level variations also remains unconstrained. However, tidal incision at Sven's Gulch (9) (Fig. 3E), suggests relative sea-level variations of the order of one decametre. This magnitude matches estimations of the amplitudes of relative sea-level variations within a Mesozoic greenhouse period, driven by 100 or 405 kyr eccentricity cycles (Aurell & Bádenas, 2004; Boulila *et al.*, 2010, 2011; Strasser *et al.*, 2012; Pellenard *et al.*, 2014). Consequently, as nine relative sea-level cycles were recorded within the Curtis Formation (Fig. 10), it is possible to bracket the time encapsulated within the Curtis Formation to between approximately 0.9 and 3.6 Ma.

CONCLUSION

The sediments of the Upper Jurassic Curtis Formation of the Colorado Plateau, Utah, USA, were deposited in a shallow-marine to marginal-marine, tidally dominated environment that responded to allocyclicly controlled fluctuations in relative sea level. Evidence of a strong tidal dominance on deposition includes bi-directional ripple cross-stratified siltstone and sandstone, as well as cross-stratified and heterolithic sandstone with flaser bedding, both of which are often arranged in cyclical tidal bundles. Tidal dominance is emphasised by a lack of fluvial influence from contemporary and neighbouring systems, and a lack of wave influence within the elongate and shallow basin, propitious to an efficient dissipation of wave energy.

The lower Curtis sediments represent early transgression of the Curtis sea and are generally contemporaneous with the neighbouring wet interdune to coastal sabkha sediments of the earthy facies of the Entrada sandstone. The lower - middle Curtis boundary represents the onset of major transgression. The middle and upper Curtis units, along with the contemporaneous deposits of the Moab Member of the Curtis Formation and Summerville Formation, represent post-major transgression deposition.

Major stratigraphic surfaces (flooding surfaces, ravinement surfaces, and regressive surfaces of marine erosion) are traceable through sediments of the lower Curtis, and upper Curtis, and their correlative continental equivalents. These surfaces are related to oscillations in relative sea level that may be connected to 100 and or 405 kyr Milankovitch cycles, although the exact causes remain equivocal. The surfaces divide the sedimentary succession into a number of packages that are governed by allocyclic process, but display internal sedimentology dominated by tidal processes.

Sediments of the middle Curtis unit are characterised exclusively by tidal facies and a lack of correlatable stratigraphic surfaces. They represent the onset of tidal amplification by resonance within the Curtis sea. The signatures of allocyclic processes within the sediments are overprinted by those of tidal currents, despite their presence in neighbouring contemporaneous deposits outside of the shallow-marine realm.

The study demonstrates that, given the right sedimentary basin geometry and conditions, the normally dominant allocyclic signatures within shallow-marine sediments related to relative sea-level oscillations may be overprinted and obscured by the usually subordinate localised autocyclic processes of the marine system, such as tides. The importance of examining shallow-marine strata in the context of the deposits of their neighbouring and contemporaneous environments, particularly in settings where the marine basin forms a small and protected embayment, is clear.

Acknowledgements

The authors of this paper would like to thank the Norwegian Research Council for their awarded COPASS grant 244049. Acknowledgements are to be extended to Dr Hannah L. Brooks, Dr Anja Sundal, Dr Miquel Poyatos-Moré, Dr Mark Mulrooney, Anna v. Yperen, and Nathan Cote for their assistance and fruitful comments, which enhanced the quality of this work. The paper is published by permission of the Executive Director, British Geological Survey (UKRI).The three anonymous reviewers who worked on an earlier version of this manuscript are to be sincerely acknowledged for their constructive observations and remarks.

Conflict of Interest

There are no conflicts of interest in the preparation or publication of this work.

REFERENCES

Ahokas, J.M., Nystuen, J.P., and **Martinius, A.W.** (2014). Depositional dynamics and sequence development in a tide-influenced marginal marine basin: Early Jurassic Neill Klinter Group, Jameson Land Basin, East Greenland. In: *From depositional systems to sedimentary successions on the Norwegian continental margin* (Eds Martinius, A.W., Ravnas, R., Howell, J., Steel, R.J., & Wonham, J.), *IAS Special Publication,* **46**, 291-338.

Alberti, M., Fürsich, F.T., and **Pandey, D.K.** (2012). The Oxfordian stable isotope record ($\delta^{18}O$, $\delta^{13}C$) of belemnites, brachiopods, and oysters from the Kachchh Basin (western India) and its potential for palaeoecologic, palaeoclimatic, and palaeogeographic reconstructions. *Palaeogeography, Palaeoclimatology, Palaeoecology*, **344**, 49-68.

Allen, J.R.L. (1968). The nature and origin of bed‐form hierarchies. *Sedimentology*, **10**, 161-182.

Anderson, T.H. (2015). Jurassic (170–150 Ma) basins: The tracks of a continental-scale fault, the Mexico-Alaska megashear, from the Gulf of Mexico to Alaska. In: *Late Jurassic Margin of Laurasia – A Record of Faulting Accommodating Plate Rotation*. *Geological Society of America Special Papers* (Eds Anderson, T.H., Didenko, A.N., Johnson, C.L., Khanchuk, A.I., and MacDonald, J.H.) , **513**, 107-188.

Anderson, O.J. and **Lucas, S.G.** (1994). Middle Jurassic stratigraphy, sedimentation and paleogeography in the southern Colorado Plateau and southern High Plains. In: *Mesozoic Systems of the Rocky Mountain Region, USA* (Eds Caputo, M.V., Peterson, J.A. and Franczyk, K.J.), The Rocky Mountain Section SEPM (Society for Sedimentary Geology), Denver, 299-314.

Aurell, M., and **Bádenas, B.** (2004). Facies and depositional sequence evolution controlled by high-frequency sea-level changes in a shallow-water carbonate ramp (late Kimmeridgian, NE Spain). *Geological Magazine*, **141**, 717-733.

Barnard, P.L., Hanes, D.M., Rubin, D.M., and **Kvitek, R.G.** (2006). Giant sand waves at the mouth of San Francisco Bay. *Eos, Transactions American Geophysical Union*, **87***,* 285-289.

Baas, J.H., Best, J.L., and **Peakall, J.** (2016). Predicting bedforms and primary current stratification in cohesive mixtures of mud and sand. *Journal of the Geological Society*, **173**, 12-45.

Bjerrum, C.J. and **Dorsey, R.J.** (1995) Tectonic controls on deposition of Middle Jurassic strata in a retroarc foreland basin, Utah‐Idaho trough, western interior, United States. *Tectonics*, **14**, 962-978.

de Boer, W.P., Roos, P.C., Hulscher, S.J., and **Stolk, A.** (2011). An idealized model of tidal dynamics in semi-enclosed basins: The effects of a mega-scale sand extraction trench in the North Sea. *Coastal Engineering Proceedings*, **1**, 1-7.

Bostock, J., and **Riley, H.T.** (1855). Pliny the Elder. *The Natural History*, 16:1(2).

Boulila, S., Galbrun, B., Hinnov, L.A., Collin, P.Y., Ogg, J.G., Fortwengler, D., and **Marchand, D.** (2010). Milankovitch and sub-Milankovitch forcing of the Oxfordian (Late Jurassic) terres noires formation (SE France) and global implications. *Basin Research*, **22**, 717-732.

Boulila, S., Galbrun, B., Miller, K.G., Pekar, S.F., Browning, J.V., Laskar, J., and **Wright, J.D.** (2011). On the origin of Cenozoic and Mesozoic "third-order" eustatic sequences. *Earth-Science Reviews*, **109**, 94-112.

Boyd, R., Dalrymple, R., and **Zaitlin, B.A.** (1992). Classification of clastic coastal depositional environments. *Sedimentary Geology*, **80**, 139-150.

Brenner, R.L. and **Peterson, J.A.** (1994). Jurassic sedimentary history of the northern portion of the Western Interior Seaway, USA. In: *Mesozoic Systems of the Rocky Mountain Region, USA* (Eds Caputo, M.V., Peterson, J.A. and Franczyk, K.J.), The Rocky Mountain Section SEPM (Society for Sedimentary Geology), Denver, 233-272.

Bonaventura, X., Sima, A.A., Feixas, M., Buckley, S.J., Sbert, M., and **Howell, J.A.** (2017). Information measures for terrain visualization. *Computers & Geosciences*, **99**, 9-18.

Buckley, S., Ringdal, K., Dolva, B., Naumann, N., and **Kurz, T.** (2017). LIME: 3D visualisation and interpretation of virtual geoscience models. *EGU General Assembly Conference Abstracts*, **19**, p. 15952.

Bump, A.P. and **Davis, G.H.** (2003). Late Cretaceous – early Tertiary Laramide deformation of the northern Colorado Plateau, Utah and Colorado. *Journal of Structural Geology*, **25**, 421-440.

Burgess, P.M., and **Prince, G.D.** (2015). Non-unique stratal geometries: implications for sequence stratigraphic interpretations. *Basin Research*, **27**, 351-365.

856 **Caputo, M.V.** and **Pryor, W.A.** (1991). Middle Jurassic tide- and wave-influenced coastal facies and
857 paleography, upper San Rafael Group, east-central Utah. *Utah Geological Association,* **19**, 9-27.

858 **Catuneanu O.** (2006). *Principles of Sequence Stratigraphy*. Amsterdam, Elsevier, 375 pp..

859 **Catuneanu, O., Abreu, V., Bhattacharya, J.P., Blum, M.D., Dalrymple, R.W., Eriksson, P.G.,**
860 **Fielding, C.R., Fisher, W.L., Galloway, W.E., Gibling, M.R., Giles, K.A., Holbrook, J.M., Jordan,**
861 **R., Kendall, C.G.St.C, Macurda, B., Martinsen, O.J., Mial, A.D., Neal, J.E., Nummedal, D., Pomar,**
862 **L., Posamentier, H.W., Pratt, B.R., Sarg, J.F., Shanley, K.W., Steel, R.J., Strasser, A., Tucker,**
863 **M.E.,** and **Winker, C.** (2009). Towards the standardization of sequence stratigraphy. *Earth-Science*
864 *Reviews*, **92**, 1-33.

865 **Carr-Crabaugh, M.** and **Kocurek, G.** (1998). Continental sequence stratigraphy of a wet eolian
866 system: a key to relative sea-level change. *Society for Sedimentary Geology, Special Publication,* **59**,
867 213-228.

868 **Cecil, C.B.** (2003). The concept of autocyclic and allocyclic controls on sedimentation and
869 stratigraphy, emphasizing the climatic variable. In: *Climate Controls on Stratigraphy* (Eds Cecil, C.B.,
870 Edgar, N.T.), *SEPM (Society for Sedimentary Geology) Special Publication*, **77**, 13-20.

871 **Chumakov, N.M., Zakharov, V.A.,** and **Rogov, M.A.** (2014). Did an ice sheet exist in Northeast Asia
872 at the Middle-Late Jurassic boundary? (Critical remarks on the article by Y. Donnadieu et al.(2011)"A
873 mechanism for brief glacial episodes in the Mesozoic greenhouse"). *Stratigraphy and Geological*
874 *Correlation*, **22**, 655-658.

875 **Crabaugh, M.,** and **Kocurek, G.** (1993). Entrada Sandstone—an example of a wet eolian system. In:
876 *The dynamics and environmental context of eolian sedimentary systems* (Eds Pye, K.), *London*
877 *Geological Society Special Publications,* **72**, 103-126.

878 **Condon, S.M.,** and **Huffman Jr, A.C.** (1988). Revisions in nomenclature of the middle Jurassic
879 Wanakah Formation, northwestern New Mexico and northeastern Arizona. *U.S. Geological Survey*
880 *Bulletin*, **1633-A**, A1-A12.

881 **Dalrymple, R.W., Zaitlin, B.A.,** and **Boyd, R**. (1992). Estuarine facies models: conceptual basis and
882 stratigraphic implications: perspective. *Journal of Sedimentary Research*, **62**, 1130-1146.

Dickinson, W.R., and **Gehrels, G.E.** (2003). U–Pb ages of detrital zircons from Permian and Jurassic eolian sandstones of the Colorado Plateau, USA: paleogeographic implications. *Sedimentary Geology*, **163**, 29-66.

Dickinson, W.R., and **Gehrels, G.E.** (2009). U-Pb ages of detrital zircons in Jurassic eolian and associated sandstones of the Colorado Plateau—evidence for transcontinental dispersal and intraregional recycling of sediment. *Geological Society of America Bulletin*, **121**, 408-433.

Dickinson, W.R., and **Gehrels, G.E.** (2010). Insights into North American paleogeography and paleotectonics from U–Pb ages of detrital zircons in Mesozoic strata of the Colorado Plateau, USA. *International Journal of Earth Sciences*, **99**, 1247-1265.

Doelling, H.H. (2001). *Geologic map of the Moab and eastern part of the San Rafael Desert 30′ x 60′ quadrangles, Grand and Emery Counties, Utah, and Mesa County, Colorado*. Utah Geological Survey Map 180, 3 plates, scale 1:100,000.

Doelling, H.H., Sprinkel, D.A., Kowallis, B.J., and **Kuehne, P.A. (2013)**. Temple Cap and Carmel Formations in the Henry Mountains Basin, Wayne and Garfield Counties, Utah. In: *The San Rafael Swell and Henry Mountains Basin-geologic centerpiece of Utah* (Eds Morris, T.H., and Ressetar, R.), *Utah Geological Association Publication*, **42**, 279-318.

Doelling, H.H., Kuehne, P.A., Willis, G.C., and **Ehler, J.B.** (2015). *Geologic map of the San Rafael Desert 30′ x 60′ quadrangle, Emery and Grand Counties, Utah*. Utah Geological Survey, Map 267DM, scale 1:62,500.

Donnadieu, Y., Dromart, G., Goddéris, Y., Pucéat, E., Brigaud, B., Dera, G., Dumas, C., and **Olivier, N.** (2011). A mechanism for brief glacial episodes in the Mesozoic greenhouse. *Paleoceanography and Paleoclimatology*, **26**, 1-10.

Dossett, T. S. (2014). *The first 40Ar/39Ar ages and tephrochronologic framework for the Jurassic Entrada Sandstone in central Utah*. Brigham Young University, Utah, master thesis, 1-46.

Dromart, G., Garcia, J.P., Picard, S., Atrops, F., Lécuyer, C., and **Sheppard, S.M.F.** (2003). Ice age at the Middle–Late Jurassic transition?. *Earth and Planetary Science Letters*, **213**, 205-220.

Fan, D. (2012). Open-coast tidal flats. In: *Principles of tidal sedimentology* (Eds Davis, R.A., Jr., and Dalrymple, R.W.), Dordrecht, Netherlands, Springer Science and Business Media, 187–229.

911 **Fertl, W.H., Chilingarian, G.V.,** and **Yen, T.F.** (1982). Use of natural gamma ray spectral logging in
912 evaluation of clay minerals. *Energy Sources*, **6**(4), 335-360.

913 **Getty, P.R.** and **Hagadorn, J.W.** (2009). Palaeobiology of the Climactichnites
914 tracemaker. *Palaeontology*, **52**, 753-778.

915 **Gilluly, J.** and **Reeside Jr., J.B.** (1928). Sedimentary rocks of the San Rafael Swell and some
916 adjacent areas in eastern Utah. *U.S. Geological Survey, Professional Paper ,***150-D***,* 61-110.

917 **Godin, G.** (1993). On tidal resonance. *Continental Shelf Research*, **13**, 89-107.

918 **Gregoire, G., Ehrhold, A., Le Roy, P., Jouet, G.,** and **Garlan, T.** (2016). Modern morpho-
919 sedimentological patterns in a tide-dominated estuary system: the Bay of Brest (west Britanny,
920 France). *Journal of Maps*, **12**, 1152-1159.

921 **Gugliotta, M., Flint, S.S., Hodgson, D.M.,** and **Veiga, G.D.** (2016). Recognition criteria,
922 characteristics and implications of the fluvial to marine transition zone in ancient deltaic deposits
923 (Lajas Formation, Argentina). *Sedimentology*, **63**, 1971-2001.

924 **Halland, E.K., Bjørnestad, A., Magnus, C., Riis, F., Meling, I.M., Tørneng Gjeldvik, I., Tappel, I.M.,**
925 **Mujezinović, J., Bjørheim M., Rød, R.S.,** and **Pham, V.T.H.** (2014). *CO_2 storage atlas—Norwegian*
926 *continental shelf*. Stavanger, Norway, Norwegian Petroleum Directorate.

927 **Harris, P.T., Heap, A.D., Bryce, S.M., Porter-Smith, R., Ryan, D.A.,** and **Heggie, D.T.** (2002).
928 Classification of Australian clastic coastal depositional environments based upon a quantitative
929 analysis of wave, tidal, and river power. *Journal of Sedimentary Research*, **72**, 858-870.

930 **Haq, B.U., Hardenbol, J.,** and **Vail, P.R.** (1987). Chronology of fluctuating sea levels since the
931 Triassic. *Science*, **235**, 1156-1167.

932 **Heyman, O.,** (1983). Distribution and structural geometry of faults and folds along the northwestern
933 Uncompahgre Uplift, western Colorado and eastern Utah. In: *Northern Paradox Basin-Uncompahgre*
934 *Uplift* (Eds Averett, W.), Grand Junction Geological Society, Grand Junction, Colorado, 45-57.

935 **Hintze, L.F.** (1980). *Geologic map of Utah.* Utah Geological and Mineral Survey, scale 1:250,000, 2
936 sheets.

937 **Hintze, L.F.** and **Kowallis, B.J.** (2009). *Geologic history of Utah.* Provo, Utah, Brigham Young
938 University Studies. 225 pp.

939 **Imlay, R.W.** (1947). Marine Jurassic of Black Hills Area, South Dakota and Wyoming. *American*
940 *Association of Petroleum Geologists Bulletin*, **31**, 227-273.

941 **Imlay, R. W.** (1952). Marine origin of Preuss sandstone of Idaho, Wyoming, and Utah. *American*
942 *Association of Petroleum Geologists Bulletin*, **36**, 1735-1753.

943 **Imlay, R.W.** (1980). Jurassic paleobiogeography of the conterminous United States in its continental
944 setting. *U.S. Geological Survey Professional Paper*, **1062**, 1-134.

945 **Kocurek, G.** (1988). First-order and super bounding surfaces in eolian sequences—bounding
946 surfaces revisited. *Sedimentary Geology*, **56**, 193-206.

947 **Kocurek, G.** (2003). Limits on extreme eolian systems: Shara of Mauritania and Jurassic Navajo
948 Sandstone examples. In: *Extreme depositional environments: mega end members in geologic time*
949 (Eds Chan, M.A., and Archer, A.W.), *Geological Society of America Special Paper*, **370**, 43-52.

950 **Kocurek, G.** and **Havholm, K.G.** (1993). Eolian sequence stratigraphy: A conceptual framework. In:
951 *Siliciclastic Sequence Stratigraphy: Recent Developments and Applications* (Eds Weimer, P., and
952 Posamentier, H.W.) *, American Association of Petroleum Geologists, Memoir,* **58**, 393–410.

953 **Kocurek, G.** and **Lancaster, N.** (1999). Aeolian system sediment state: theory and Mojave Desert
954 Kelso dune field example. *Sedimentology*, **46**, 505-515.

955 **Kocurek, G., Martindale, R.C., Day, M., Goudge, T.A., Kerans, C., Hassenruck - Gudipati, H.J.,**
956 **Mason, J., Cardenas, B.T., Petersen, E., Mohrig, D., Aylward, D.S., Hughes, C.M.,** and **Nazworth,**
957 **C.M.** (2018). Antecedent aeolian dune topographic control on carbonate and evaporite facies: Middle
958 Jurassic Todilto Member, Wanakah Formation, Ghost Ranch, New Mexico, USA. *Sedimentology*, 1-
959 30.

960 **Kreisa, R.D.** and **Moiola, R.J.** (1986). Sigmoidal tidal bundles and other tide-generated sedimentary
961 structures of the Curtis Formation, Utah. *Geological Society of America Bulletin*, **97**, 381-387.

962 **Kvale, E.P.** (2012). Tidal constituents of modern and ancient tidal rhythmites: criteria for recognition
963 and analyses. In: *Principles of Tidal Sedimentology* (Eds Davis, R.A., Jr., and Dalrymple, R.W.),
964 Springer Science and Business Media, Dordrecht, Netherlands, 1-17.

965 **Levander, A., Schmandt, B., Miller, M.S., Liu, K., Karlstrom, K.E., Crow, R.S., Lee, C.-T.A.,** and
966 **Humphreys, E.D.** (2011). Continuing Colorado plateau uplift by delamination-style convective
967 lithospheric downwelling. *Nature*, **472***,* 461-465.

968 **Li, M.Z., Shaw, J., Todd, B.J., Kostylev, V.E.,** and **Wu, Y.** (2014). Sediment transport and
969 development of banner banks and sandwaves in an extreme tidal system: Upper Bay of Fundy,
970 Canada. *Continental Shelf Research*, **83**, 86-107.

971 **Longhitano, S.G., Mellere, D., Steel, R.J.,** and **Ainsworth, R.B.** (2012). Tidal depositional systems
972 in the rock record: a review and new insights. *Sedimentary Geology*, **279**, 2-22.

973 **Lucas, S.G.** (2014). Lithostratigraphy of the Jurassic San Rafael Group from Bluff to the Abajo
974 Mountains, southeastern Utah: Stratigraphic relationships of the Bluff Sandstone. *Volumina Jurassica*,
975 **12**, 55-68.

976 **Mansfield, G.R.** and **Roundy, P.V.** (1916). Revision of the Beckwith and Bear River Formations of
977 southeastern Idaho. *U.S. Geological Survey Professional Paper*, **98**, 75-84.

978 **Martinius, A.W.** and **Gowland, S.** (2011). Tide‐influenced fluvial bedforms and tidal bore deposits
979 (late Jurassic Lourinhã Formation, Lusitanian Basin, Western Portugal). *Sedimentology*, **58**, 285-324.

980 **Martinius, A.W., Ringrose, P.S., Brostrøm, C., Elfenbein, C., Næss, A.,** and **Ringås, J.E.** (2005).
981 Reservoir challenges of heterolithic tidal sandstone reservoirs in the Halten Terrace, mid-Norway.
982 *Petroleum Geoscience*, **11**, 3-16.

983 **McMullen, S.K., Holland, S.M.,** and **O'Keefe, F.R.** (2014). The occurrence of vertebrate and
984 invertebrate fossils in a sequence stratigraphic context: the Jurassic Sundance Formation, Bighorn
985 Basin, Wyoming, USA. *Palaios*, **29**, 277-294.

986 **Midtkandal, I.,** and **Nystuen, J.P.** (2009). Depositional architecture of a low-gradient ramp shelf in an
987 epicontinental sea: the lower Cretaceous of Svalbard. *Basin Research*, **21**, 655-675.

988 **Mitchum, R.J., Vail, P.R.,** and **Thompson, S. III.** (1977) The depositional sequence as a basic unit
989 for stratigraphic analysis. *In:* Payton, C.E., (ed.), *Seismic Stratigraphy: Applications to Hydrocarbon*
990 *Exploration*, *American Association of Petroleum Geologists Memoir,* **26**, 205-212.

991 **Mountney, N.P.** (2006). Periodic accumulation and destruction of aeolian erg sequences in the
992 Permian Cedar Mesa Sandstone, White Canyon, southern Utah, USA. *Sedimentology,* **53**, 789-823.

Mountney, N.P. (2012). A stratigraphic model to account for complexity in aeolian dune and interdune successions. *Sedimentology*, **59***,* 964-989.

Murray, K.E., Reiners, P.W., and **Thomson, S.N.** (2016). Rapid Pliocene–Pleistocene erosion of the central Colorado Plateau documented by apatite thermochronology from the Henry Mountains. *Geology*, **44***,* 483-486.

Nelson, S.T. (1997). Reevaluation of the Central Colorado plateau laccoliths in the light of new age determination. *U.S. Geological Survey Bulletin*, **2158**, 37-39.

Ogg, J.G., Ogg, G., and **Gradstein, F M.** (2016). *A Concise Geologic Time Scale: 2016*. Elsevier.

Osleger, D. (1991). Subtidal carbonate cycles: Implications for allocyclic vs. autocyclic controls. *Geology*, **19(**, 917-920.

Otto, E.P. and **Picard, M.D.** (1976). Petrology of the Entrada Sandstone (Jurassic), northeastern Utah. *In*: Hill, J.G., (ed), *Geology of the Cordilleran hingeline*. Rocky Mountain Association of Petroleum Geologists Guidebook, 231-259.

Pellenard, P., Tramoy, R., Pucéat, E., Huret, E., Martinez, M., Bruneau, L., and **Thierry, J.** (2014). Carbon cycle and sea-water palaeotemperature evolution at the Middle–Late Jurassic transition, eastern Paris Basin (France). *Marine and Petroleum Geology*, **53**, 30-43.

Peterson, F. (1994). Sand dunes, sabkhas, streams, and shallow seas: Jurassic paleography in the southern part of the Western Interior Basin. In: *Mesozoic Systems of the Rocky Mountain Region, USA* (Eds Caputo, M.V., Peterson, J.A. and Franczyk, K.J.), The Rocky Mountain Section SEPM (Society for Sedimentary Geology), Denver, 233-272.

Peterson, F. and **Pipiringos, G.N.** (1979). Stratigraphic relations of the Navajo Sandstone to Middle Jurassic formations, southern Utah and northern Arizona*. U.S. Geological Survey Professional Paper*, **1035-B**, 1-43.

Pipiringos, G.N. and **O'Sullivan, R.B.** (1978). Principal unconformities in Triassic and Jurassic rocks, western interior United States: a preliminary survey. *U.S. Geological Survey, Professional Paper,* **1035-A**, 1-29.

Pipiringos, G.N., and **Imlay, R.W.** (1979). Lithology and subdivisions of the Jurassic Stump Formation in southeastern Idaho and adjoining areas. *U.S. Geological Survey Professional Paper,* **1035-C**, 1-25.

Reynaud, J.Y. and **Dalrymple, R.W.** (2012). Shallow-marine tidal deposits. In: *Principles of Tidal Sedimentology* (Eds Davis, R.A., Jr., and Dalrymple, R.W.), Springer Science and Business Media, Dordrecht, Netherlands, 335-369.

Roos, P.C. and **Schuttelaars, H.M.** (2011). Influence of topography on tide propagation and amplification in semi-enclosed basins. *Ocean Dynamics*, **61**, 21-38.

Schulz, M., and **Schäfer - Neth, C.** (1997). Translating Milankovitch climate forcing into eustatic fluctuations via thermal deep water expansion: a conceptual link. *Terra Nova*, **9**, 228-231.

Scott, R.B., Harding, A.E., Hood, W.C., Cole, R.D., Livaccari, R.F., Johnson, J.B., Shroba, R.R., and **Dickerson, R.P.** (2001). *Geologic map of Colorado National Monument and adjacent areas, Mesa County, Colorado*. U.S. Geological Map I-2740, 40 p., 1 plate, scale 1:24,000.

Shaw, J., Todd, B.J., and **Li, M.Z.** (2014). Geologic insights from multibeam bathymetry and seascape maps of the Bay of Fundy, Canada. *Continental Shelf Research*, **83**, 53-63.

Sprinkel, D.A., Doelling, H.H., Kowallis, B.J., Waanders, G., and **Kuehne, P.A.** (2011a). Early results of a study of Middle Jurassic strata in the Sevier fold and thrust belt, Utah. In*: Sevier Thrust Belt: Northern and Central Utah and Adjacent Areas* (Eds Sprinkel, D.A., Yonkee, W.A., and Chidsey, T.C., Jr.), *Utah Geological Association, Publication,* **40**, 151-172.

Sprinkel, D.A., Kowallis, B.J., and **Jensen, P.H.** (2011b). Correlation and age of the Nugget Sandstone and Glen Canyon Group, Utah. In*: Sevier Thrust Belt: Northern and Central Utah and Adjacent Areas* (Eds Sprinkel, D.A., Yonkee, W.A., and Chidsey, T.C., Jr.),*Utah Geological Association Publication*, **40**, 131-149.

Strasser, A., Pittet, B., Hillgärtner, H., and **Pasquier, J. B.** (1999). Depositional sequences in shallow carbonate-dominated sedimentary systems: concepts for a high-resolution analysis. *Sedimentary Geology*, **128**, 201-221.

Strasser, A., Vedrine, S., and **Stienne, N.** (2012). Rate and synchronicity of environmental changes on a shallow carbonate platform (Late Oxfordian, Swiss Jura Mountains). *Sedimentology*, **59**, 185-211.

Sullivan, K.R., Kowallis, B.J., and **Mehnert, H.H.** (1991). Isotopic ages of igneous intrusions in southeastern Utah – Evidence for a mid-Cenozoic Reno–San Juan magmatic zone. *Brigham Young University Geology Studies*, **37**, 139-144.

Svendsen, J.B. and **Hartley, N.R.** (2001). Comparison between outcrop-spectral gamma ray logging and whole rock geochemistry: Implications for quantitative reservoir characterisation in continental sequences. *Marine and Petroleum Geology*, **18**, 657-670.

Sztanó, O. and **de Boer, P.L.** (1995). Basin dimensions and morphology as controls on amplification of tidal motions (the Early Miocene North Hungarian Bay). *Sedimentology*, **42**, 665-682.

Tape, C.H., Cowan, C.A., and **Runkel, A.C.** (2003). Tidal-bundle sequences in the Jordan Sandstone (Upper Cambrian), southeastern Minnesota, USA: evidence for tides along inboard shorelines of the Sauk epicontinental sea. *Journal of Sedimentary Research*, **73**, 354-366.

Thorman, C.H. (2011). The Elko orogeny – A major tectonic event in eastern Nevada–western Utah. In*: Sevier Thrust Belt: Northern and Central Utah and Adjacent Areas* (Eds Sprinkel, D.A., Yonkee, W.A., and Chidsey, T.C., Jr.), *Utah Geological Association Publication,* **40**, 117-129.

Todd, B.J., Shaw, J., Li, M.Z., Kostylev, V.E., and **Wu, Y.** (2014). Distribution of subtidal sedimentary bedforms in a macrotidal setting: The Bay of Fundy, Atlantic Canada. *Continental Shelf Research*, **83**, 64-85.

Trudgill, B.D. (2011). Evolution of salt structures in the northern Paradox Basin: Controls on evaporite deposition, salt wall growth and supra‐salt stratigraphic architecture. *Basin Research*, **23**, 208-238.

Valenza, J.M. (2016). Redbeds of the Upper Entrada Sandstone, Central Utah: Facies Analysis and Regional Implications of Interfingered Sabkha and Fluvial Terminal Splay Sediments. Brigham Young University, Utah, master thesis, 1-54.

Vallis, G.K. (2017). *Atmospheric and oceanic fluid dynamics*. Cambridge University Press. 745 pp.

Wang, P. (2012). Principles of Sediment Transport Applicable in Tidal Environments. In: *Principles of Tidal Sedimentology* (Eds Davis, R.A., Jr., and Dalrymple, R.W.), Springer Science and Business Media, Dordrecht, Netherlands, 19-34.

Wang, D., Liu, Q., and **Lv, X.** (2014). A study on bottom friction coefficient in the Bohai, Yellow, and East China Sea. *Mathematical Problems in Engineering*, 2014, 1-7.

1075 **Walker, R.G.** (1992). Facies, facies models and modern stratigraphic concepts. *In*: Walker, R.G., and
1076 James, N.P. (eds.), *Facies models: response to sea-level change*, *Geological Association of Canada*,
1077 1-14.

1078 **Westoby, M.J., Brasington, J., Glasser, N.F., Hambrey, M.J.,** and **Reynolds, J.M.** (2012).
1079 'Structure-from-Motion'photogrammetry: A low-cost, effective tool for geoscience
1080 applications. *Geomorphology*, **179**, 300-314.

1081 **Wilcox, W.T.** and **Currie, B.** (2008). Sequence Stratigraphy of the Jurassic Curtis, Summerville, and
1082 Stump Formations, Eastern Utah and Northwest Colorado. In: *Hydrocarbon Systems and Production*
1083 *in the Uinta Basin, Utah* (Eds Longman, M.W., and Morgan, C.D.), *Rocky Mountain Association of*
1084 *Geologists and Utah Geological Association Publication,* **37**, 9-41.

1085 **Witkind, I.J.** (1988). *Geologic map of the Huntington 30' X 60' quadrangle, Carbon, Emery, Grand,*
1086 *and Uintah Counties, Utah.* U.S. Geological Survey, Miscellaneous Investigations Series Map I-1764,
1087 scale 1:100,000.

1088 **Wierzbowski, H., Dembicz, K.,** and **Praszkier, T.** (2009). Oxygen and carbon isotope composition of
1089 Callovian–Lower Oxfordian (Middle–Upper Jurassic) belemnite rostra from central Poland: A record of
1090 a Late Callovian global sea-level rise? *Palaeogeography, Palaeoclimatology, Palaeoecology*, **283**,
1091 182-194.

1092 **Yonkee, W.A.** and **Weil, A.B.** (2015). Tectonic evolution of the Sevier and Laramide belts within the
1093 North American Cordillera orogenic system. *Earth-Science Reviews*, **150**, 531-593.

1094 **Yoshida, S., Steel, R.J.,** and **Dalrymple, R.W.** (2007). Changes in depositional processes—an
1095 ingredient in a new generation of sequence-stratigraphic models. *Journal of Sedimentary Research*,
1096 **77**, 447-460.

1097 **Zuchuat, V., Sleveland, A.R.N., Sprinkel, D.A., Rimkus, A., Braathen, A.,** and **Midtkandal, I.**
1098 (2018). New insights on the impact of tidal currents on a low-gradient, semi-enclosed, epicontinental
1099 basin—the Curtis Formation, east-central Utah, USA. *Geology of the Intermountain West*, **5**, 131-165.

1100 **Zuchuat, V., Midtkandal, I., Poyatos-Moré, M., da Costa, S., Halvorsen, K., Cote N., Sundal, A.,**
1101 and **Braathen, A.** (in press). Composite Unconformities in Low-Gradient Transitional Settings: the J-3
1102 Unconformity and the Curtis Formation, East-Central Utah, USA. *The Journal of Sedimentary*
1103 *Research.*

FIGURE CAPTIONS

Fig. 1. Modern day, tide-dominated coastline environments (modified from Boyd *et al.*, 1992; Harris *et al.*, 2002; Fan, 2012).

Fig. 2. (A-B) Maps of the study area. Green dots represent visited localities where the Curtis Formation crops out, while the red dots illustrate its absence. Each code number on the map refers to a specific locality in the attached table (Geological units after Hintze, 1980; Witkind, 1988; Doelling, 2001; Doelling *et al.*, 2013; Sprinkel *et al.*, 2011a; 2011b; and Doelling *et al.*, 2015; Tectonic setting after Heyman, 1983; Thorman, 2011). GJ: Grand Junction, GR: Green River, HKS: Hanksville, MB: Moab, SRS: San Rafael Swell. (C) Schematic lithostratigraphic column showing a correlation between the San Rafael Swell area, east-central Utah, and Ghost Ranch, in northern New Mexico (Doelling, 2001; Doelling *et al.*, 2015; Kocurek *et al.*, 2018; Zuchuat *et al.,* 2018;). Note that the contemporaneous character between the Entrada Sandstone and the lower Curtis, as well as between the middle Curtis, upper Curtis, Moab Member, and Summerville Formation is not shown in this lithostratigraphic display.

Table 1. Facies description for the Entrada Sandstone, Curtis Formation, and Summerville Formation.

Table 2. Facies associations for the Entrada Sandstone, Curtis Formation, and Summerville Formation.

Fig. 3. Summary panel of the Facies Associations (FA) cropping out within the study area. (A) Example of wet coastal aeolian dunes of FA 1a (Entrada Sandstone, Slick Rock Member). (B) Amalgamated aeolian coastal dunes within the fine-grained, marginal marine earthy facies of FA1b (Entrada Sandstone). Note the bleached horizon directly below the dunes. Geologist for scale. (C) High-energy upper shoreface to beach deposits, with rip-up clasts and occasional mud drapes. Note the loaded and eroded irregular geometry of the J-3 Unconformity. (D) Typical stacking architecture of subtidal mud- (FA 3a) and sand-dominated heterolithic flat deposits (FA 3b). (E) Major tidal incision observed at Sven's Gulch, carved during a short-lived regressive phase within Parasequence 2. The dark-red arrow points at a boulder of Entrada Sandstone within a matrix of FA 3b sand-dominated deposits. Note also the ravinement of Parasequence 2 deposits during the transgressive phase of Parasequence 3, followed by the by the development of a regressive and erosive, subtidal channel complex (FA 4b). (F) Mini sag basin generated by the collapse of FA 3b deposits, as FA 4a sand-rich

subtidal to supratidal sandflat was being deposited. (G) Two incision phases of FA 4b subtidal channel. (H) Bidirectional tidal inlets (red and blue contours), and a third south-westward laterally accreting tidal channel (green contour) within a subtidal to intertidal flat surrounding environment (FA 5). The respective migration direction of these three bedforms is colour-coded on the rose-diagram, whereas the black line on the diagram illustrates the outcrop orientation. (I) Conformable contact between the underlying FA 5 subtidal to intertidal channel-dune-flat complex, grading into the thinner and finer-grained FA 6 upper subtidal to intertidal deposits, which are conformably overlain by FA 8 supratidal deposits of the Summerville Formation. (J) Five aeolian sequences recorded in the Moab Member of the Curtis Formation. (K) Close-up images of FA 8 supratidal deposits displaying regular episodes of marine flooding (white sandstone beds).

Fig. 4. (A) N-S-W oriented correlation panel along the NW margin of the San Rafael Swell, and the correlative spatial distribution of facies associations across the Curtis basin. The datum corresponds to the Major Transgressive Surface (MTS). (B) Rose diagrams displaying the palaeocurrent measurements for the lower Curtis (FA 2, FA 3, and FA 4), the middle Curtis (FA 5), and the upper Curtis-Summerville Formation intervals (FA 6 and FA 8).

Fig. 5. Duma Point sedimentary section and associated cyclical gamma-ray log. The thorium/uranium (Th/U) values generally fall below 7 at approximately 5, which suggest a more prominent marine origin for these sediments, rather than a fully continental provenance (Fertl *et al.,* 1982). The Morrison Formation is shaded as it is not of interest for this study. See Fig. 2 for section location.

Fig. 6. (A) Three different conglomeratic deposits observable within the lower Curtis unit. Note the waxing-waning bundle arrangement of the upper gravelly channel and the absence of similar structure in the gravelly dunes. (B-C) Close-up of the basal flash flood pebbly conglomerate, overlain by a gravelly dune. (D) lateral migration of a sinuous subtidal, gravelly channel. Note its concave up, erosive base and flat upper surface (see Fig. 10 for detail architectural arrangement of that subtidal channel). (E) Gravelly dune, arranged in waxing-waning bundles, migrating over subtidal, mud-dominated heterolithic flat deposits (FA 3a).

Fig. 7. Common tide-dominated and tidally-modulated bedforms present in the Curtis Formation. See Facies Table 1 for codes. (A) Bi-directional rippled cross-stratified sandstone (Facies R). (B) Heterolithic siltstone and sandstone with lenticular (LB) and wavy bedding (WB) (Facies L, M). (C) Bi-directional rippled cross-stratified sandstone with episodic climbing ripples (Facies R). (D) Tangential

cross-stratified gravelly sandstone (Facies H), thought to result from tidally-reworked flash flood deposits, migrating over a sole of mud- to sand-dominated heterolithic deposits (FA 3). (E) Heterolithic siltstone and sandstone with wavy and flaser bedding (FB) (Facies M, N), arranged in rhythmic tidal bundle. (F) Tangential cross-stratified sandstone (Facies C), with rippled reactivation surfaces, mud drapes and rip-up mud clasts. (). Cross-stratified sandstone arranged in well-defined rhythmic tidal bundles (Facies P). (H) Heterolithic sandstone with flaser bedding (Facies N), arranged in rhythmic tidal bundle. (I) Organic-rich (OM) toesets of a cross-stratified sandstone arranged in well-defined rhythmic tidal bundles (TB) (Facies P).

Fig. 8. E-W oriented correlation panel across the marine part and the aeolian Moab Member of the Curtis Formation. The datum corresponds to the Major Transgressive Surface (MTS). Note that the five, cyclical aeolian sequences identified in the Moab Member of the Curtis Formation suggest that the contemporaneous Summerville Formation could have undergone, and most probably underwent, similar cycles as it was being deposited.

Fig. 9. Summary basinal history for the Entrada-Curtis-Summerville interval: (A) As the Curtis sea transgression had started but had not yet flooded the study area, the paralic deposits of the earthy facies of the Entrada Sandstone developed contemporaneously to the aeolian dunes of the Slick Rock Member of the Entrada Sandstone. (B-D) As the Curtis sea kept transgressing, the sea experienced allocyclicly-driven relative sea-level variations, leading to the development of three parasequences in the lower Curtis, each bounded by traceable flooding surfaces. (E) The Major Transgression flooded the entire study area (and beyond), and marks the base of the middle Curtis. (F-G) As the Curtis sea started regressing, the middle Curtis was coexisting with the shallower upper Curtis, the sabkha deposits of the Summerville Formation, and the aeolian dunes of the Moab Member of the Curtis Formation. The development of the paralic domain and coastal dunes was dictated by allocyclically-driven relative sea-level variations. The shallow-marine part of the system was under the influence of tidal resonance, leading to the dominance of autocyclic processes, and the overprinting of the relative sea-level signature in the sedimentary record. (H) The Curtis sea kept regressing, and the sediment supply necessary to the survival of the aeolian dunes of the Moab Member of the Curtis Formation was shut down, and the coastal dune field was terminated, as the entire study area was occupied by the paralic deposits of the Summerville Formation.

Fig. 10. Comparison between the relative sea-level signal recorded by the marine part (Sven's Gulch, left red dot on the map), the paralic neighbouring systems at Duma Point (middle red dot on the map), and the aeolian Moab Member of the Curtis Formation (Big Pinto Mesa, right red dot on the map), illustrating the overwriting of allocyclic signals by the tide-dominated system once it entered in resonance, accompanied by the deposition of the middle Curtis, whereas the contemporaneous aeolian deposits kept recording such allocyclicly-forced relative sea-level variations. The paralic succession also shows obvious cyclical floodings, but the accurate relationship between these observed cycles with the neighbouring systems remains puzzling. See Fig. 11 for illustration of uplift phases. RSME = Regressive Surface of Marine Erosion; FS = Flooding Surface; MTS = Major Transgressive Surface; MFS = Maximum Flooding Surface; TST = Transgressive System Tract; HST = High Stand System Tract.

Fig. 11. (A) Photogrammetric model of Cedar Mountain showing the earthy facies of the Entrada Sandstone, the erosive relief developed at its top, as well as the lower and middle Curtis strata overlying the J-3 Unconformity. (B-C) Vertically exaggerated interpreted model, which illustrates the impact of both allocyclic and autocyclic forcing on the system as the lower Curtis was developing. Allocyclic forcing: The angular relationship between the different strata indicates that a first tilting of the Entrada Sandstone strata occurred prior to the deposition of Parasequence 1 deposits, a second one occurred before Parasequence 3 developed, and the last one preceded the Major Transgression. Further, the effect of relative sea-level variations, accompanied by the shift of the FAs belt, resulted in the development of the three parasequences. Autocyclic forcing: The minor spatio-temporal energy variations, as well as the WSE-ENE laterally migrating subtidal channel (pink-purplish tones) illustrate best the intrinsically dynamic behaviour of the tide-dominated system, but its multi-story incision-amalgamation also testifies of a potential impact of external forcing over the system. This contrasts with the middle Curtis' system and its behaviour, which was impacted and developed quasi exclusively as a response of autocyclic forcing.

Fig. 12. Models representing the spatial distribution of the different FA across and idealised Curtis-like basin during the lower Curtis, as well as the middle-upper Curtis intervals, and their correlative energy level's spatial distribution within the system, both before and after the system entered in tidal resonance once the basin threshold dimension was reached. After Sztanó and de Boer (1995), the transgressing Curtis sea is suggested to have entered at least two other phases of tidal resonance

1222 before reaching its maximal extent of ca. 800 km. Note the coarsening trend from the distal parts of
1223 the basin and towards the shoreline in the lower Curtis, with the replacement of the mud-dominated
1224 FA 3a deposits, by FA 3b's and FA 4a's coarser-grained and cleaner sediments. Palaeogeographic
1225 Map ©2014 Colorado Plateau Geosystems Inc.

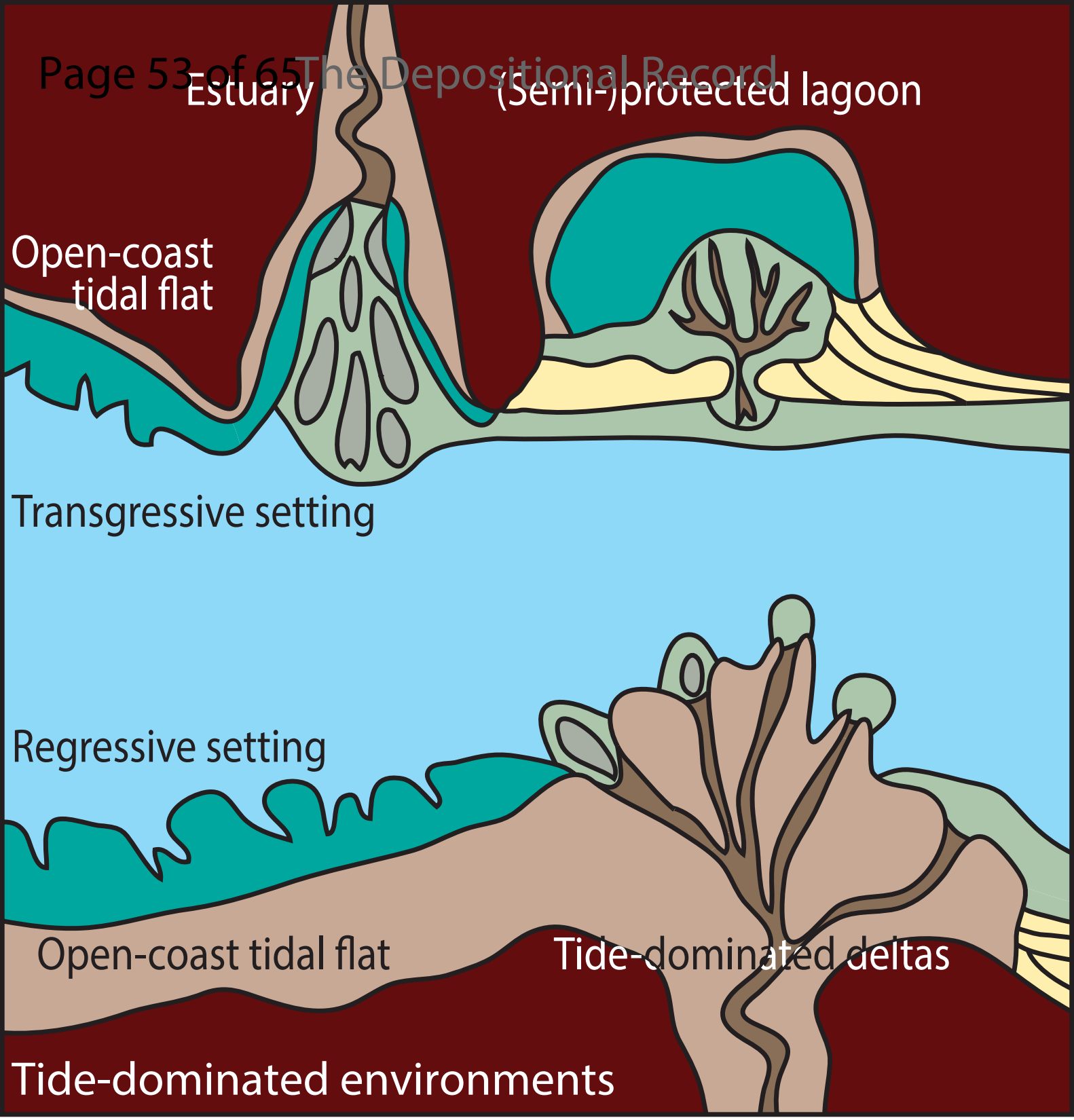

Depositional environments

- Sub- to supratidal heterolithic sandflat
- Sub- to intertidal heterolithic mudflat
- Inter- to supratidal marsh
- Barrier and beach deposits
- Sandy tidal bars and mouth bars
- Fluvial and tidal channels

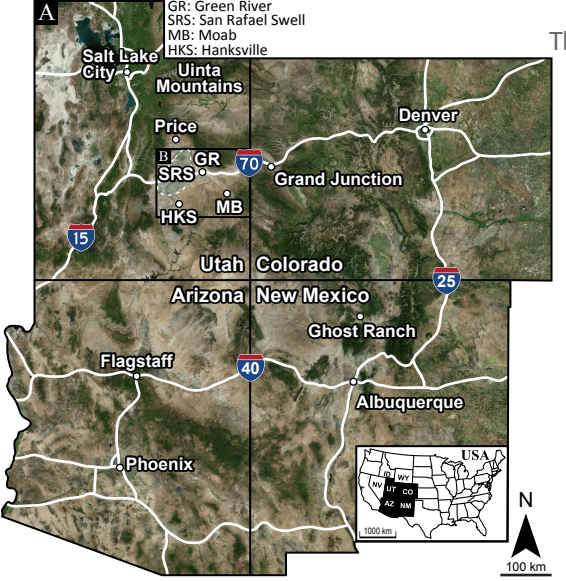

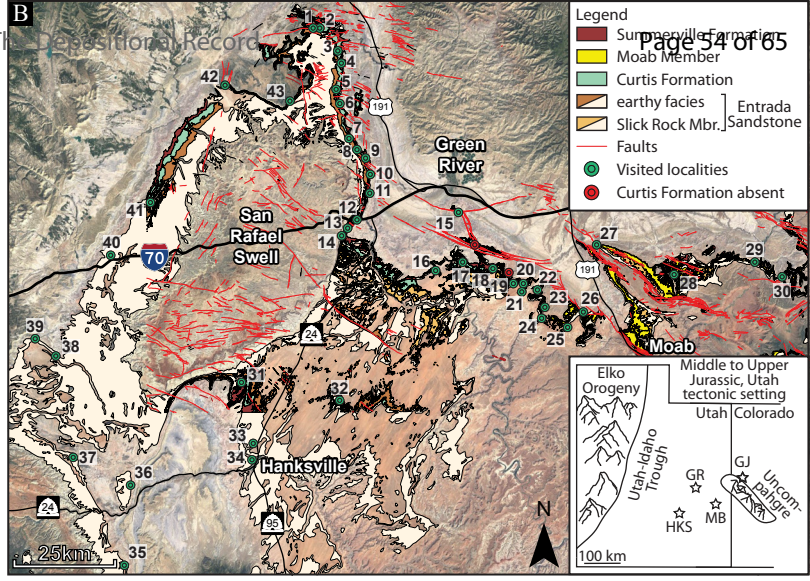

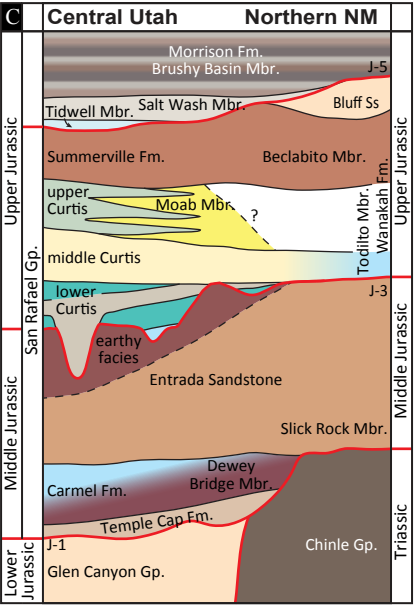

Log N°	Log name	UTM - coordinates		
		Grid	Easting	Northing
1	Sulphur Canyon	12 S	538598	4354691
2	Stove Gulch East	12 S	541150	4354677
3	Humbug Flats East	12 S	545496	4349054
4	Neversweat Wash	12 S	546582	4345984
5	Middle Canyon	12 S	545582	4340631
6	Dry Mesa	12 S	546370	4336290
7	Curtis Point	12 S	549241	4328385
8	Wet Gulch	12 S	550874	4325353
9	Sven's Gulch	12 S	552531	4323706
10	Smith's Cabin	12 S	553584	4319583
11	Rabbit Gulch	12 S	553369	4314960
12	Interstate 70	12 S	550457	4308362
13	Shadscale Mesa	12 S	548962	4306456
14	Uneva Mine Canyon	12 S	547594	4304403
15	Crystal Geyser	12 S	575060	4310623
16	Lower San Rafael Rd	12 S	570049	4295643
17	Ruby Ranch Meandre	12 S	576420	4298161
18	Ruby Ranch Road	12 S	583113	4296930
19	Duma Point	12 S	588894	4293333
20	Horse Flies Gulch	12 S	590606	4293184
21	Dune Mesa	12 S	590620	4290953
22	Ten Mile Rd	12 S	594368	4291828

Log N°	Log name	UTM - coordinates		
		Grid	Easting	Northing
23	Petrified Tree Gulch	12 S	596564	4287509
24	Dubinky Well Rd	12 S	595351	4284912
25	Safari Road	12 S	601764	4282137
26	Bartlett Wash	12 S	605257	4286436
27	Salt Valley	12 S	608768	4302663
28	Lost Spring Canyon	12 S	624118	4294979
29	Dewey Bridge	12 S	647467	4298329
30	Big Pinto Mesa	12 S	654182	4294917
31	Goblin Valley	12 S	522572	4269001
32	Little Flat Top	12 S	544488	4266008
33	Hanksville Airport	12 S	526141	4254218
34	Hanksville	12 S	525317	4248736
35	Notom Ranch	12 S	492291	4226559
36	Cainville Airstrip	12 S	495813	4244029
37	L. South Desert Ov.	12 S	481839	4250657
38	LCD the Two Towers	12 S	477493	4275207
39	LCD Road Cut	12 S	472428	4279105
40	Salt Wash View Area	12 S	490555	4298727
41	Sid and Charley	12 S	500015	4311719
42	Lower Cedar Mt Rd	12 S	518557	4340815
43	Cedar Mountain	12 S	535782	4337326

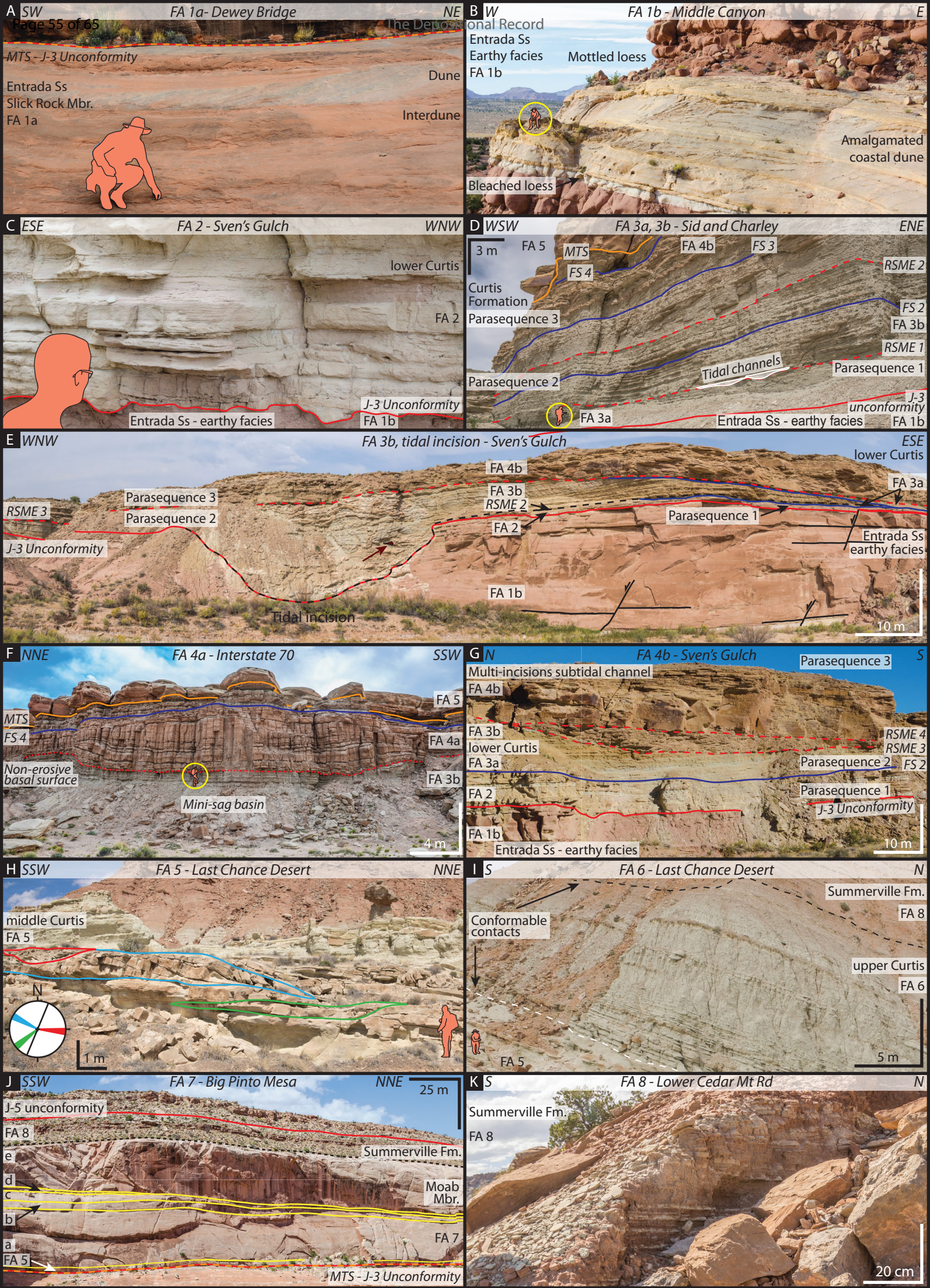
A SW FA 1a- Dewey Bridge NE
MTS - J-3 Unconformity
Entrada Ss
Slick Rock Mbr.
FA 1a
Dune
Interdune
B W FA 1b - Middle Canyon E
Entrada Ss
Earthy facies
FA 1b
Mottled loess
Amalgamated
coastal dune
Bleached loess
C ESE FA 2 - Sven's Gulch WNW
lower Curtis
FA 2
J-3 Unconformity
Entrada Ss - earthy facies
FA 1b
D WSW FA 3a, 3b - Sid and Charley ENE
3 m
FA 5
MTS
FS 4
FA 4b
FS 3
RSME 2
Curtis
Formation
Parasequence 3
FS 2
FA 3b
RSME 1
Tidal channels
Parasequence 2
Parasequence 1
J-3
unconformity
FA 3a
Entrada Ss - earthy facies
FA 1b
E WNW FA 3b, tidal incision - Sven's Gulch ESE
lower Curtis
FA 4b
FA 3a
Parasequence 3
FA 3b
RSME 2
RSME 3
Parasequence 2
FA 2
Parasequence 1
J-3 Unconformity
Entrada Ss
earthy facies
FA 1b
Tidal incision
10 m
F NNE FA 4a - Interstate 70 SSW
FA 5
MTS
FS 4
FA 4a
Non-erosive
basal surface
FA 3b
Mini-sag basin
4 m
G N FA 4b - Sven's Gulch S
Parasequence 3
Multi-incisions subtidal channel
FA 4b
FA 3b
RSME 4
RSME 3
lower Curtis
FA 3a
Parasequence 2
FS 2
FA 2
Parasequence 1
J-3 Unconformity
FA 1b
Entrada Ss - earthy facies
10 m
H SSW FA 5 - Last Chance Desert NNE
middle Curtis
FA 5
N
1 m
I S FA 6 - Last Chance Desert N
Summerville Fm.
FA 8
Conformable
contacts
upper Curtis
FA 6
FA 5
5 m
J SSW FA 7 - Big Pinto Mesa NNE
25 m
J-5 unconformity
FA 8
Summerville Fm.
e
d
Moab
Mbr.
c
b
FA 7
a
FA 5
MTS - J-3 Unconformity
K S FA 8 - Lower Cedar Mt Rd N
Summerville Fm.
FA 8
20 cm

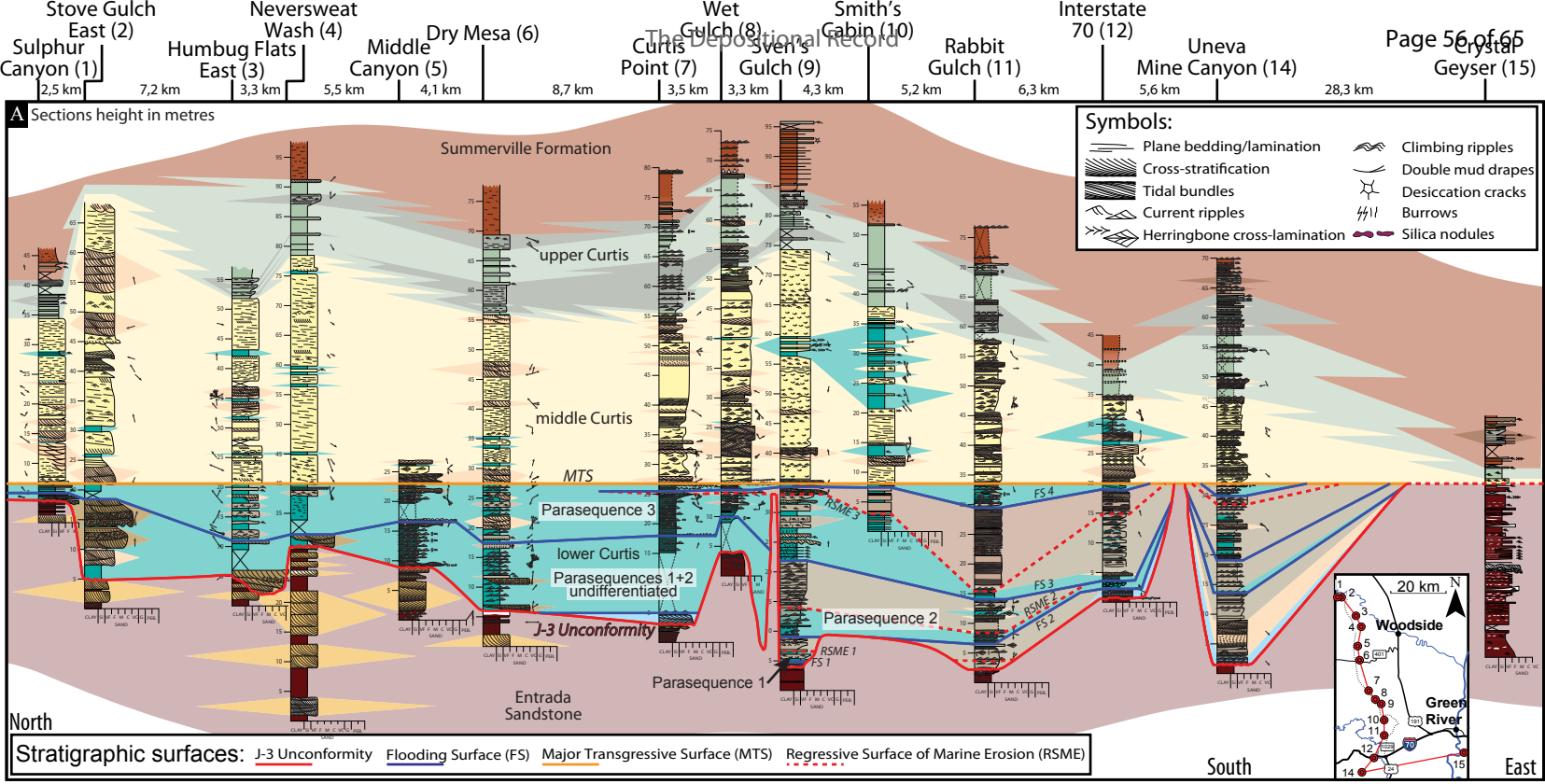

Architectural elements (logs)

- Supratidal sand flat
- Supratidal mud flat
- Upper sub- to intertidal sand-dominated heterolithic channel-flat complex
- Upper sub- to intertidal mud-dominated heterolithic flat
- Sub- to intertidal channel-dune-flat complex
- Sand-rich sub- to supratidal flat
- Tidal bundles
- Subtidal sand-dominated heterolithic flat
- Subtidal conglomeratic channels and dunes
- Subtidal mud-dominated heterolithic flat
- Upper shoreface to beach deposits
- Coastal interdunes, locally bleached or mottled
- Coastal dunes
- Coastal dunes, bleached

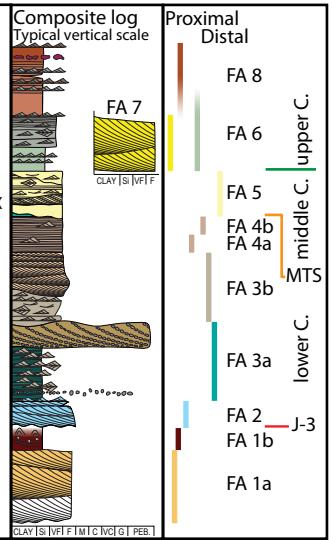

Facies Associations (correlation panel)

- FA 3b Subtidal sand-dominated heterolithic flat
- FA 3a Subtidal mud-dominated heterolithic flat
- FA 2 Upper shoreface to beach deposits
- FA 1b Earthy facies
- FA 1a Coastal dunes and Slick Rock Member
- FA 8 Supratidal flat
- FA 7 Coastal dry eolian dunes Moab Member
- FA 6 Upper sub- to intertidal heterolithic flat
- FA 5 Sub- to intertidal channel-dune-flat complex
- FA 4 Sand-rich sub- to supratidal flat and correlative tidal channel infill

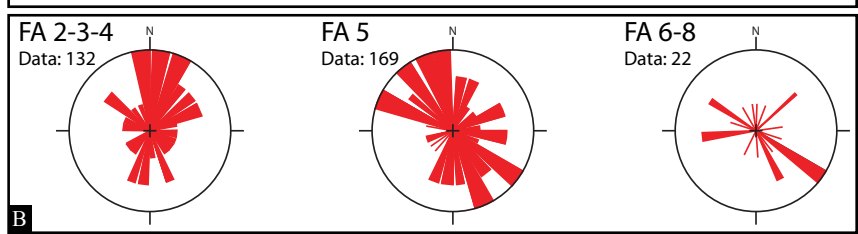

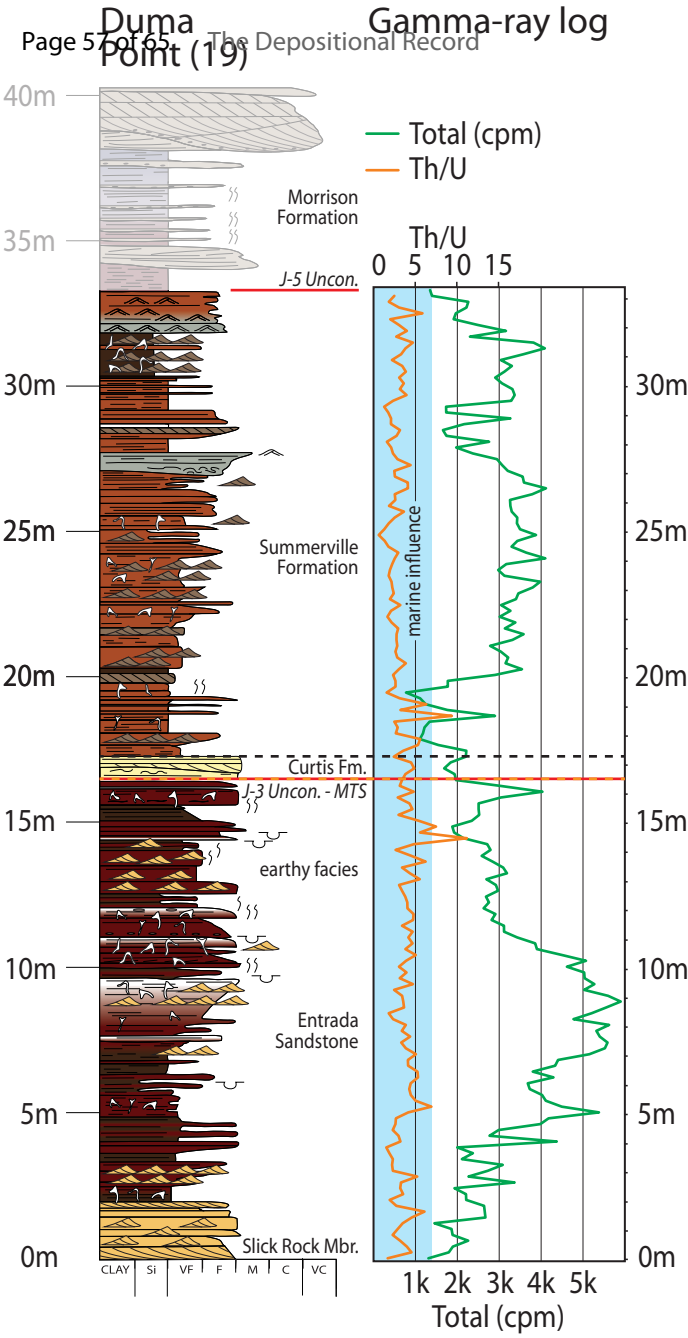

Architectural elements

- Fluvial channels
- Continental/fresh water mud flat
- Supratidal sand flat
- Supratidal mud flat
- Upper sub- to intertidal sand-dominated heterolithic channel-flat complex
- Sub- to intertidal channel-dune-flat complex
- Coastal interdunes, locally bleached or mottled
- Coastal dunes

Legend

- Planar cross-strati.
- Tangential cross-strati.
- Oscillatory current ripple
- Unidirectional current ripple
- Undifferentiated bioturbation
- Mud clasts
- Loading structures
- Mottling

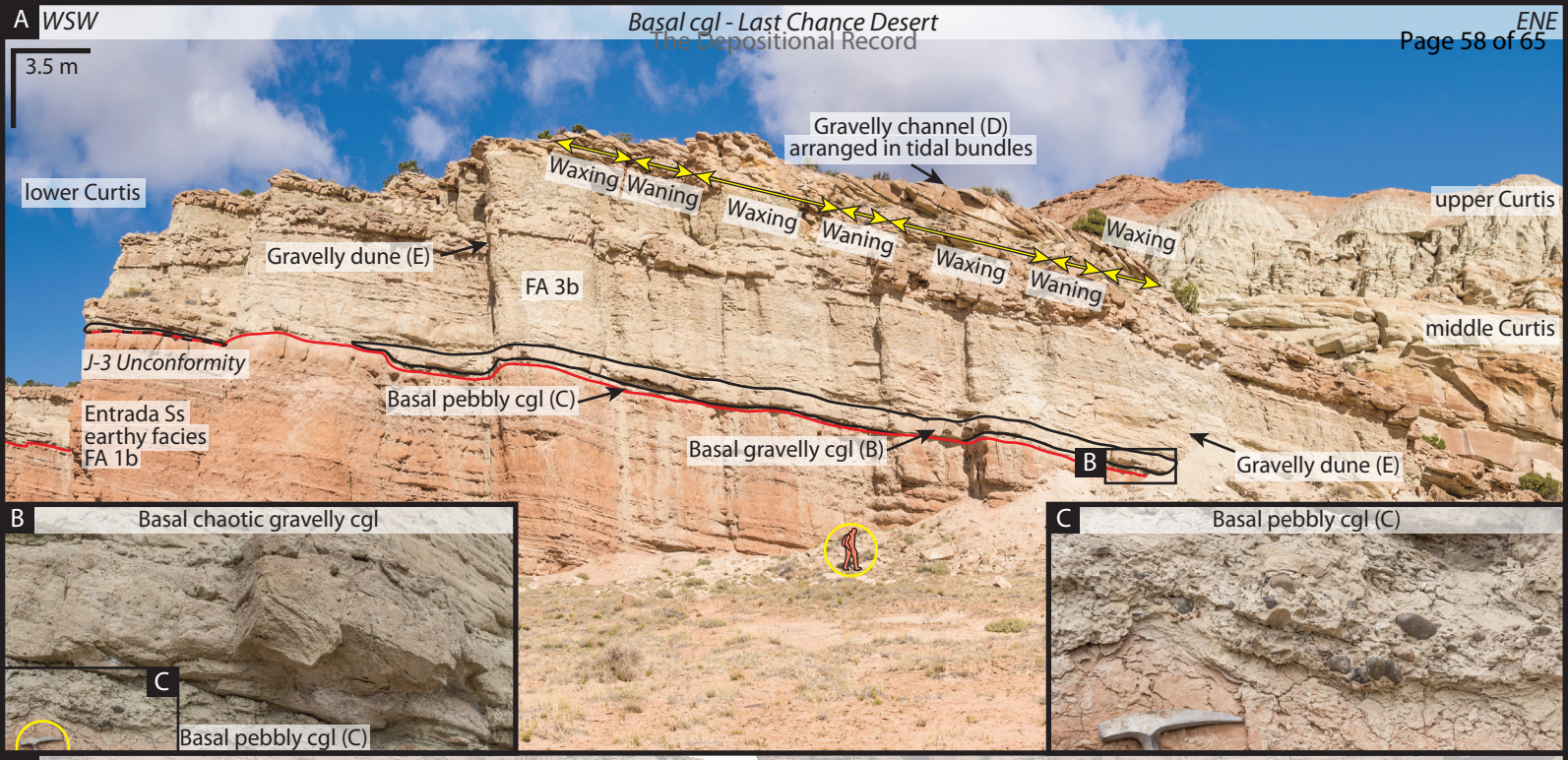
A
WSW
Basal cgl - Last Chance Desert
ENE
3.5 m
Gravelly channel (D)
arranged in tidal bundles
lower Curtis
upper Curtis
middle Curtis
Waxing
Waning
Waxing
Waning
Waxing
Waning
Waxing
Gravelly dune (E)
FA 3b
J-3 Unconformity
Basal pebbly cgl (C)
Entrada Ss
earthy facies
FA 1b
Basal gravelly cgl (B)
B
Gravelly dune (E)

B
Basal chaotic gravelly cgl
C
Basal pebbly cgl (C)

C
Basal pebbly cgl (C)

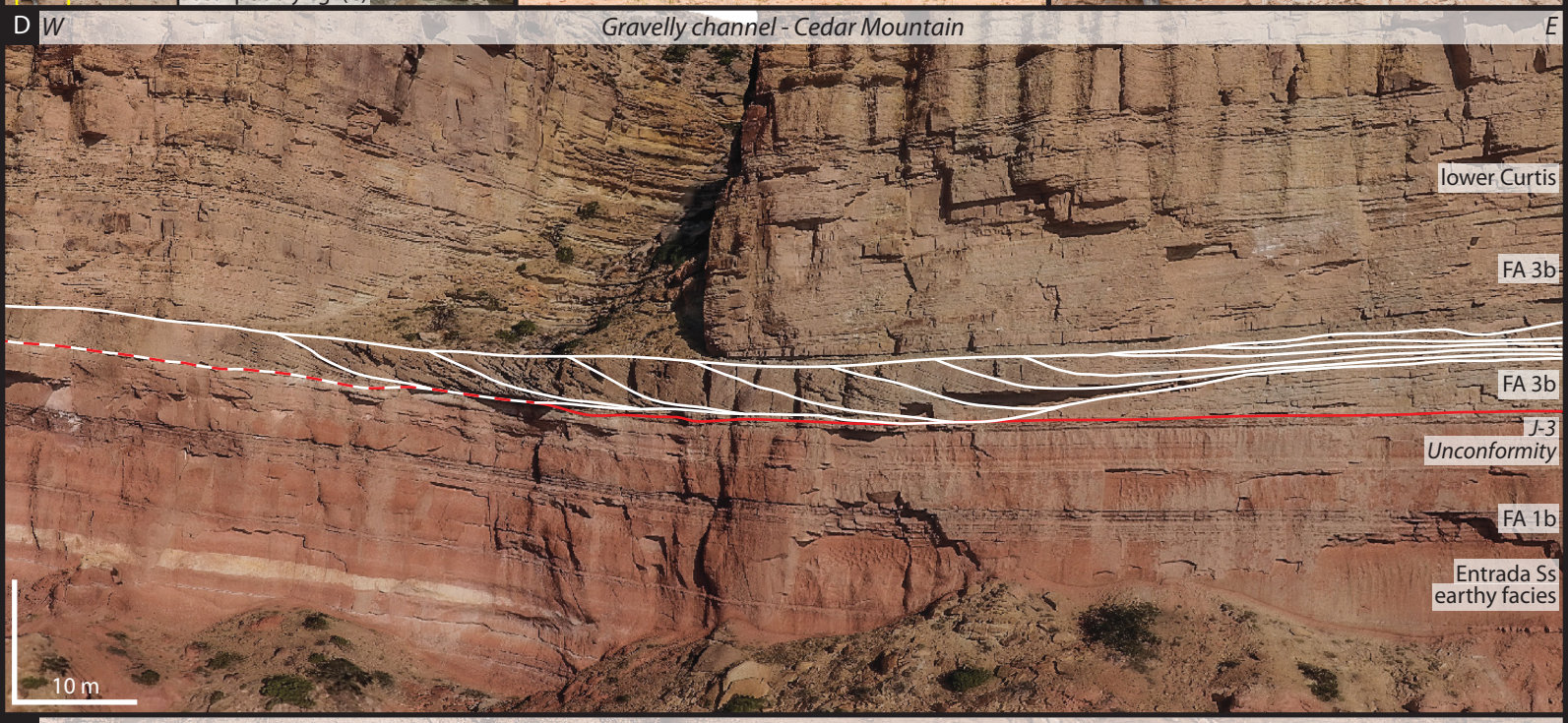
D
W
Gravelly channel - Cedar Mountain
E
lower Curtis
FA 3b
FA 3b
J-3
Unconformity
FA 1b
Entrada Ss
earthy facies
10 m

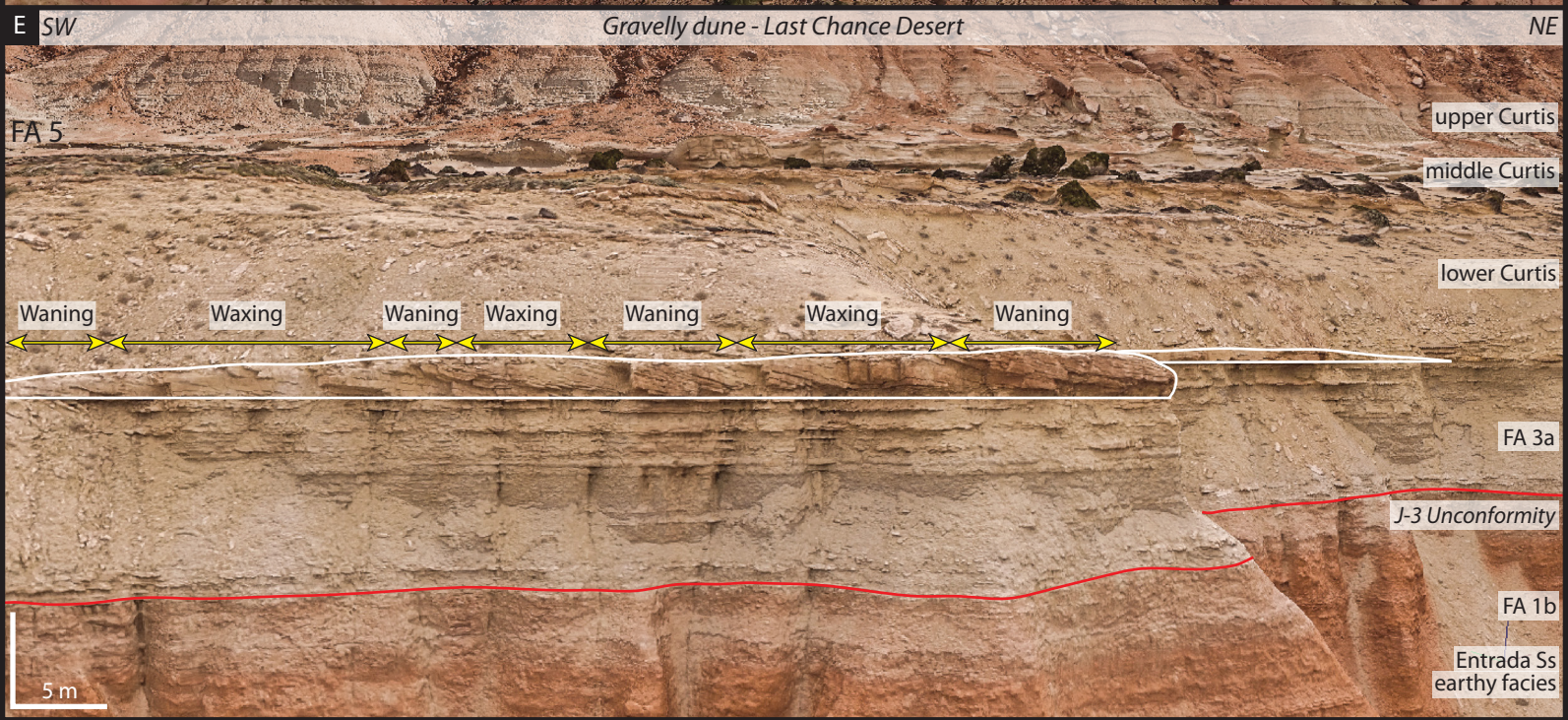
E
SW
Gravelly dune - Last Chance Desert
NE
FA 5
upper Curtis
middle Curtis
lower Curtis
Waning
Waxing
Waning
Waxing
Waning
Waxing
Waning
FA 3a
J-3 Unconformity
FA 1b
Entrada Ss
earthy facies
5 m


A
Herringbone cross-stratification - Smith's Cabin
3 cm
Facies R

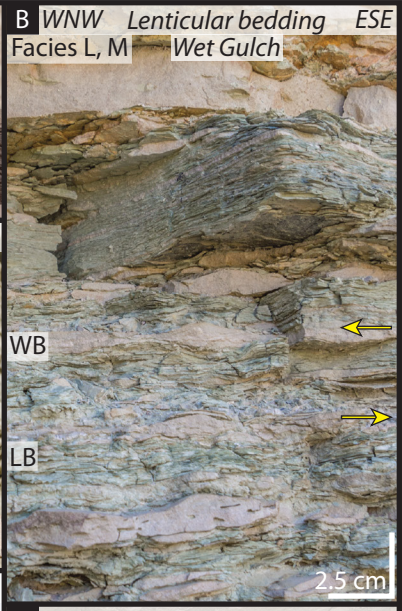
B
WNW
Lenticular bedding
ESE
Facies L, M
Wet Gulch
WB
LB
2.5 cm


C
W
Herringbone cross-stratification - Sven's Gulch
E
Facies R
Increased sediment input

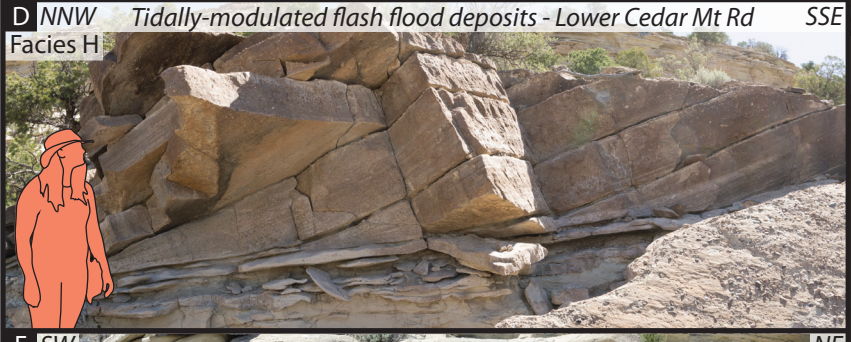
D
NNW
Tidally-modulated flash flood deposits - Lower Cedar Mt Rd
SSE
Facies H

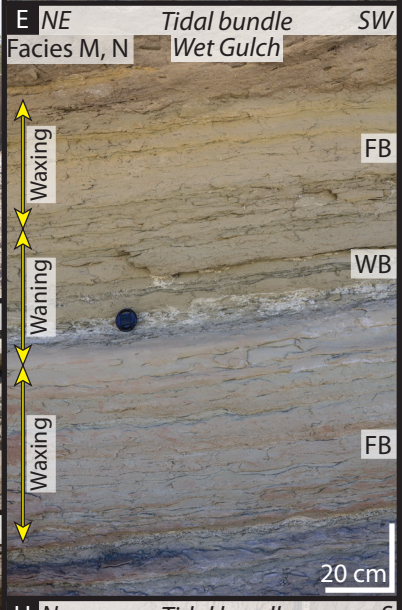
E
NE
Tidal bundle
SW
Facies M, N
Wet Gulch
Waxing
Waning
Waxing
FB
WB
FB
20 cm

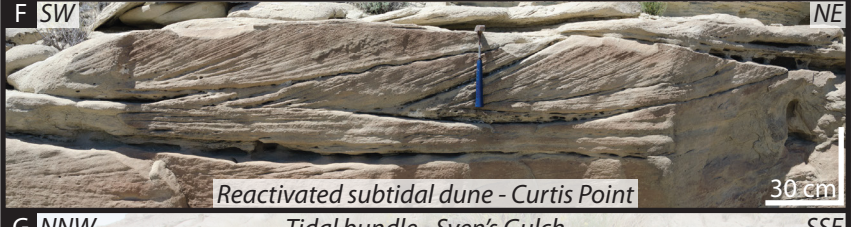
F
SW
NE
Reactivated subtidal dune - Curtis Point
30 cm


G
NNW
Tidal bundle - Sven's Gulch
SSE
Facies P
Waning
Waxing
Waning
25 cm

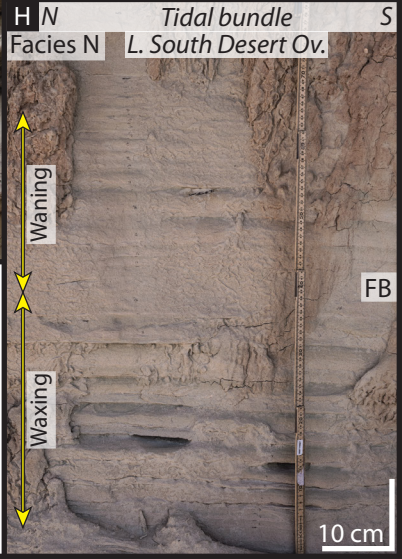
H
N
Tidal bundle
S
Facies N
L. South Desert Ov.
Waning
Waxing
FB
10 cm


I
SW
NE
Facies P
TB-toesets
OM
OM-rich tidal bundle - Wet Gulch
20 cm

Uneva Mine Canyon (14) — 23.7 km — Lower San Rafael Rd (16) — 19.1 km — Duma Point (19) — 11.7 km — Ten Mile Rd (22) — 13.4 km — Safari Road (25) — 29.2 km — Lost Spring Canyon (28) — 26.6 km — Big Pinto Mesa (30)

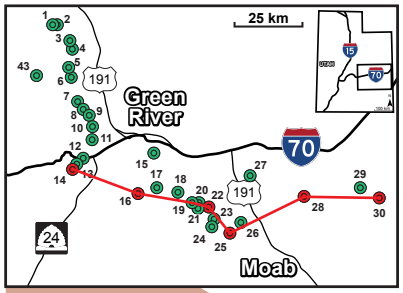

Facies Associations (correlation panel)

- FA 3b Subtidal sand-dominated heterolithic flat
- FA 3a Subtidal mud-dominated heterolithic flat
- FA 2 Upper shoreface to beach deposits
- FA 1b Earthy facies
- FA 1a Coastal dunes and Slick Rock Member
- FA 8 Supratidal flat
- FA 7 Coastal dry eolian dunes Moab Member
- FA 6 Upper sub- to intertidal heterolithic flat
- FA 5 Sub- to intertidal channel-dune-flat complex
- FA 4 Sand-rich sub- to supratidal flat

Sections height in metres

Summerville Formation

J-5 Unconformity

Morrison Formation

upper Curtis

middle Curtis

MTS

lower Curtis

FS 4

FS 3

FS 2

Entrada Sandstone earthy facies

Moab Member

e

d

c

b

a

FS 9

FS 8

FS 7

FS 6

FS 5

J-3 Unconformity

Slick Rock Member

CLAY Si VF F

West

East

Stratigraphic surfaces

- Regressive Surface of Marine Erosion (RSME)
- Flooding Surface (FS)
- Base of the Moab Member
- Major Transgressive Surface (MTS)
- J-3 Unconformity
- Base of the earty facies

Architectural elements (logs)

- Tidal bundles
- Subtidal sand-dominated heterolithic flat
- Subtidal conglomeratic channels and dunes
- Subtidal mud-dominated heterolithic flat
- Upper shoreface to beach deposits
- Coastal interdunes, locally bleached or mottled
- Coastal dunes
- Supratidal sand flat
- Supratidal mud flat
- Structureless sandstone, potential sand-stromatolite patches
- Upper sub- to intertidal sand-dominated heterolithic channel-flat complex
- Upper sub- to intertidal mud-dominated heterolithic flat
- Sub- to intertidal channel-dune-flat complex
- Sand-rich sub- to supratidal flat

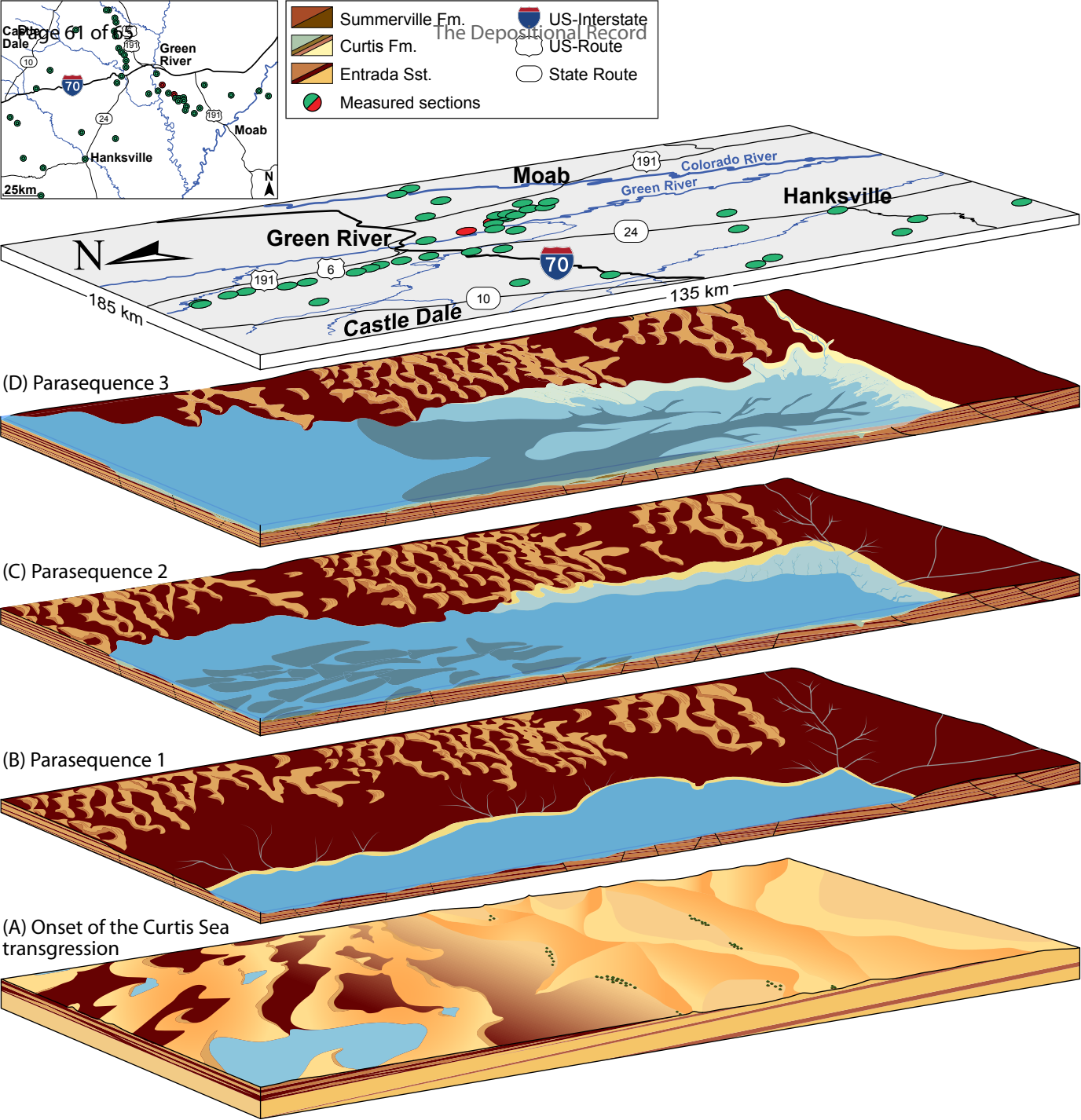

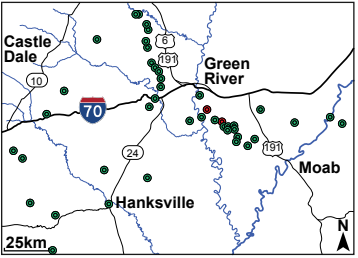

Summerville Fm.
Curtis Fm.
Entrada Sst.
Measured sections
US-Interstate
US-Route
State Route

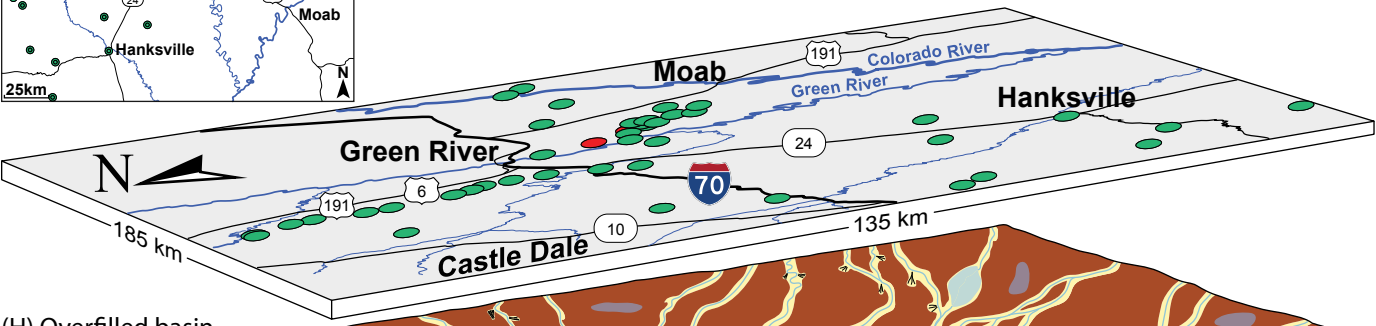

(H) Overfilled basin

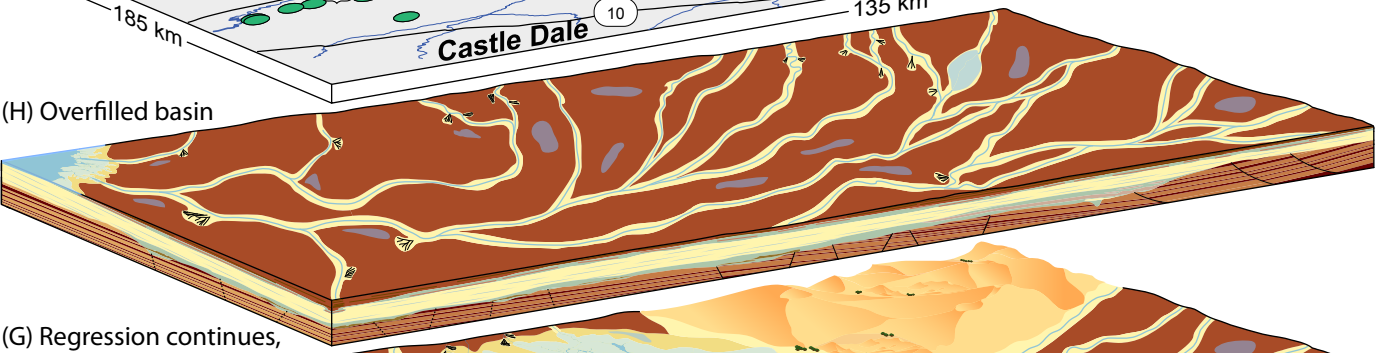

(G) Regression continues, Moab Mbr.'s max.

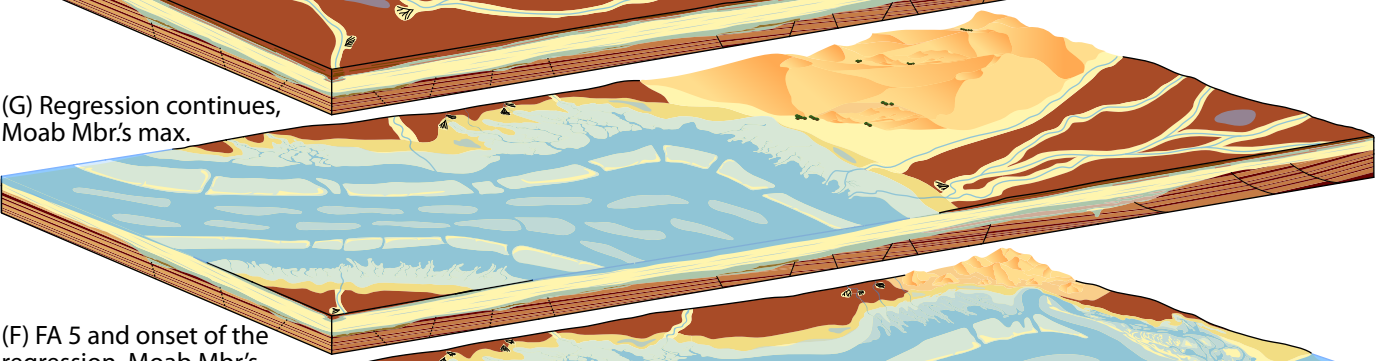

(F) FA 5 and onset of the regression, Moab Mbr.'s birth

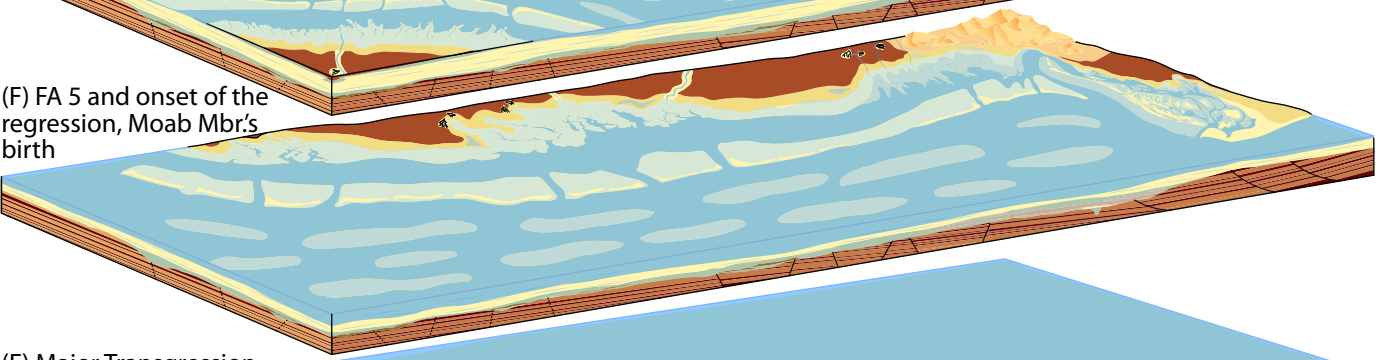

(E) Major Transgression

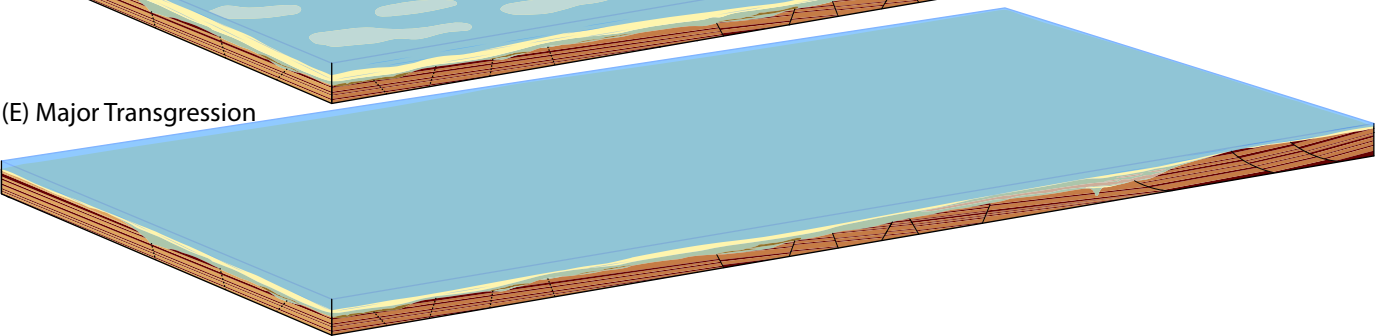

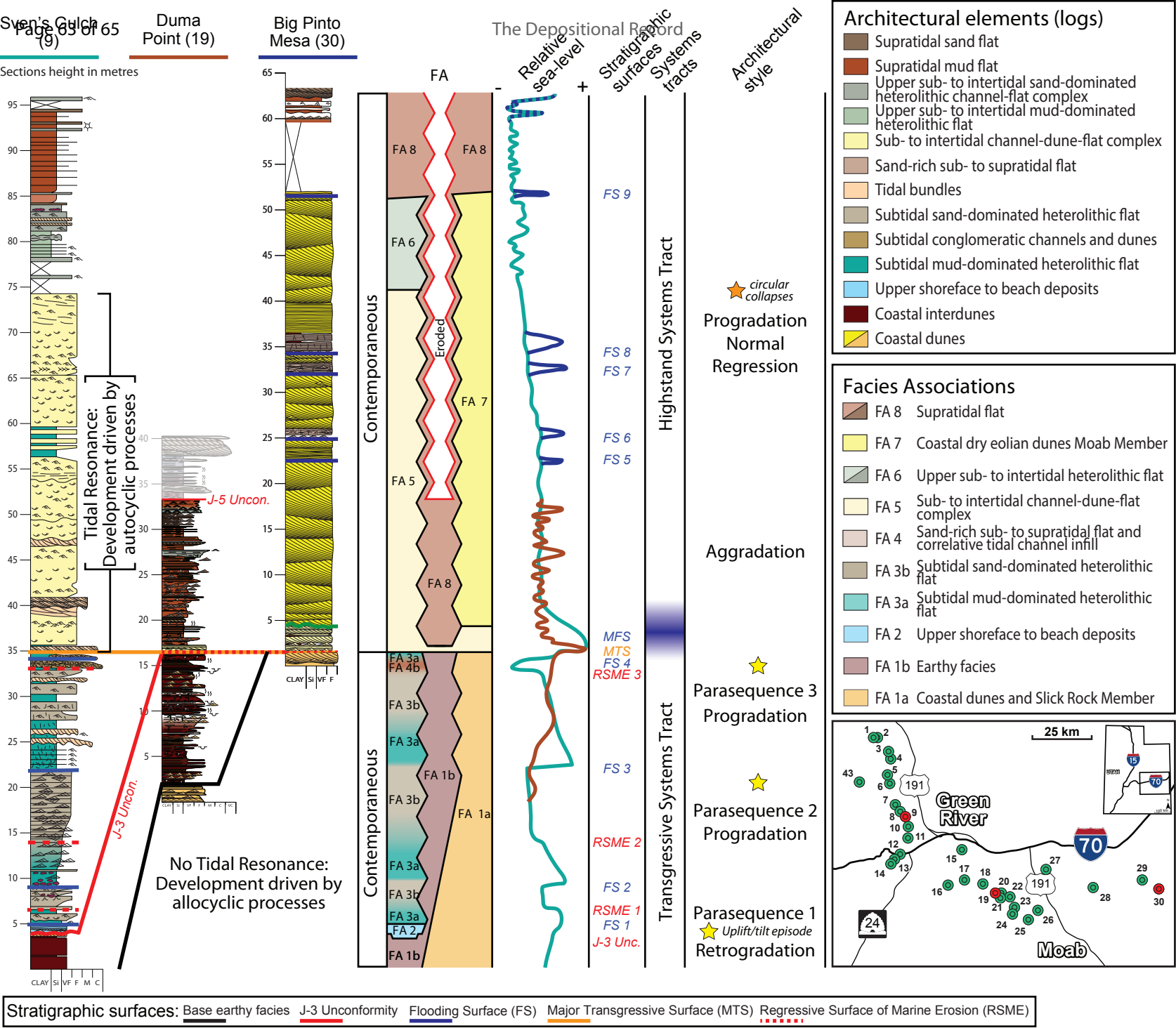

Architectural elements (logs)

- Supratidal sand flat
- Supratidal mud flat
- Upper sub- to intertidal sand-dominated heterolithic channel-flat complex
- Upper sub- to intertidal mud-dominated heterolithic flat
- Sub- to intertidal channel-dune-flat complex
- Sand-rich sub- to supratidal flat
- Tidal bundles
- Subtidal sand-dominated heterolithic flat
- Subtidal conglomeratic channels and dunes
- Subtidal mud-dominated heterolithic flat
- Upper shoreface to beach deposits
- Coastal interdunes
- Coastal dunes

Facies Associations

FA 8	Supratidal flat
FA 7	Coastal dry eolian dunes Moab Member
FA 6	Upper sub- to intertidal heterolithic flat
FA 5	Sub- to intertidal channel-dune-flat complex
FA 4	Sand-rich sub- to supratidal flat and correlative tidal channel infill
FA 3b	Subtidal sand-dominated heterolithic flat
FA 3a	Subtidal mud-dominated heterolithic flat
FA 2	Upper shoreface to beach deposits
FA 1b	Earthy facies
FA 1a	Coastal dunes and Slick Rock Member

Stratigraphic surfaces: Base earthy facies | J-3 Unconformity | Flooding Surface (FS) | Major Transgressive Surface (MTS) | Regressive Surface of Marine Erosion (RSME)

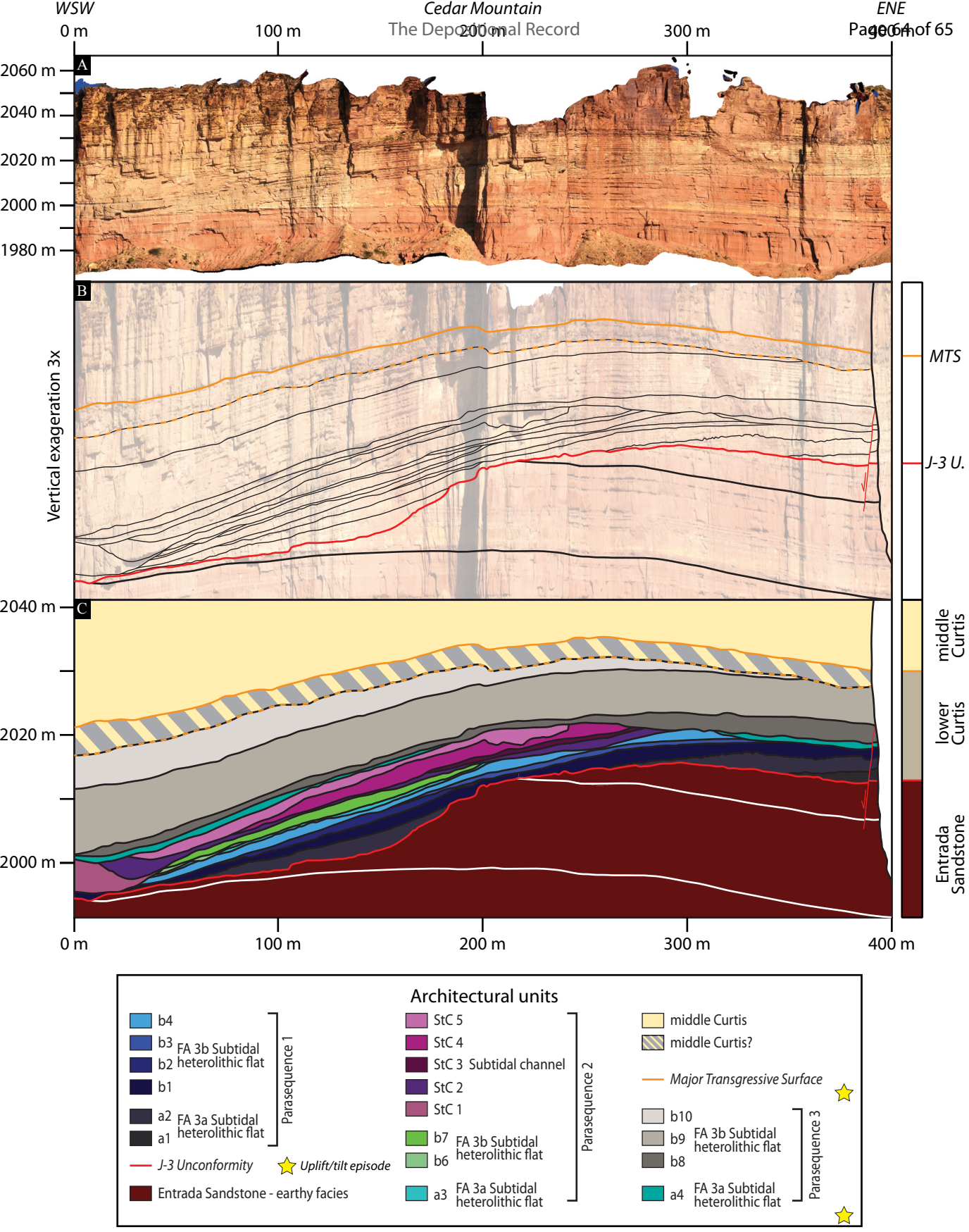
WSW
ENE
0 m
100 m
200 m
300 m
400 m
2060 m
2040 m
2020 m
2000 m
1980 m
A
B
C
Vertical exageration 3x
MTS
J-3 U.
middle Curtis
lower Curtis
Entrada Sandstone
Architectural units
b4
b3
b2
b1
FA 3b Subtidal heterolithic flat
a2
a1
FA 3a Subtidal heterolithic flat
Parasequence 1
J-3 Unconformity
Uplift/tilt episode
Entrada Sandstone - earthy facies
StC 5
StC 4
StC 3 Subtidal channel
StC 2
StC 1
b7
b6
FA 3b Subtidal heterolithic flat
a3
FA 3a Subtidal heterolithic flat
Parasequence 2
middle Curtis
middle Curtis?
Major Transgressive Surface
b10
b9
b8
FA 3b Subtidal heterolithic flat
a4
FA 3a Subtidal heterolithic flat
Parasequence 3

2. Post-Major Transgression

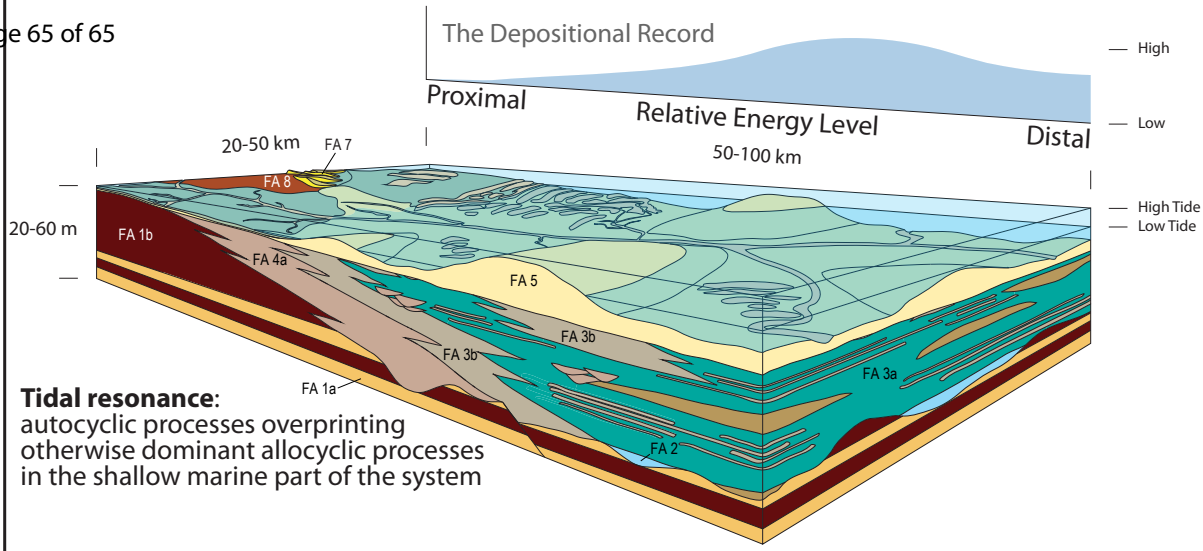

Tidal resonance:
autocyclic processes overprinting otherwise dominant allocyclic processes in the shallow marine part of the system

Major Transgression - Amplification of tidal processes as the system enters in tidal resonance

Critical basin size attained as the transgression progresses

1. Pre-Major Transgression

No tidal resonance:
Development dominated by allocyclic processes

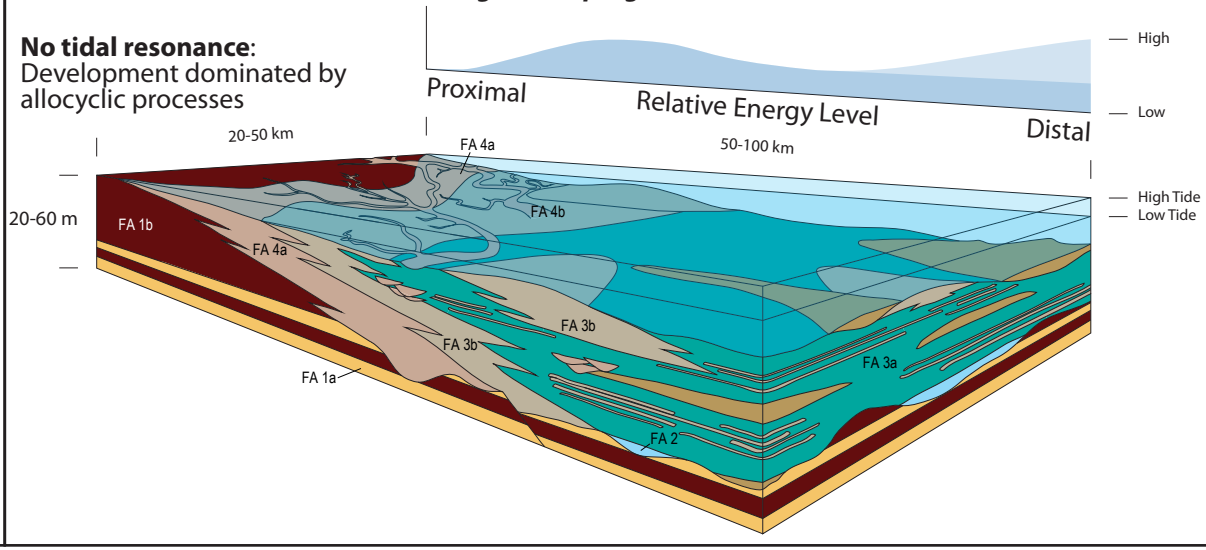

Palaeogeography Oxfordian
lower Curtis (162-161 Ma)

Curtis sea: ca. 800 km long; **water depth *d*** (Allen, 1968): $h = 0.086(d)^{1.19}$
h: average thickness of the tallest bedform, h = 3-4 m; then ***d* = 20-25 m**

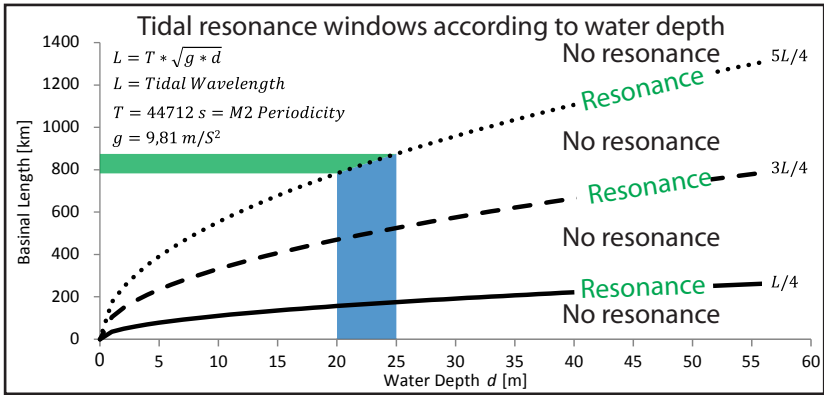

TABLE 1 - FACIES DESCRIPTION FOR THE ENTRADA SANDSTONE, CURTIS FORMATION AND SUMMERVILLE FORMATION

Facies	Description	Structures	Grain size	Interpretation	Formation
A	Cross-stratified sandstone	Unidirectional tangential cross-bedded vf-f grained sandstone, alternating grain flow and grain fall deposits, sharp base, rusty red or white, locally bleached, local occurrence of rhizoliths, varying bedform/bedform sets size, maximum individual dune thickness 15 m. Potential occurrence of counter-ripples at the toe of the foresets.	VF - F	Aeolian dune deposits, locally influenced by a dynamic and migrating water table/saturated level.	Entrada Ss Moab Mbr.
B	Plane parallel-laminated to mottled mudstone with localised evaporites	Dark red silty mudstone with pale yellow to white vf-f grained sand lenses, plane parallel-laminated to -stratified or mottled, potential bleached patches around rhizoliths, localized evaporite-rich horizons, maximum individual horizon thickness 1 cm.	Si - Cl	Aeolian interdune to coastal plain domain with occasional flooding with development of sabkha-type deposits and/or superficial vegetation.	Entrada Ss Summerville Fm.
C	Tangential cross-stratified sandstone	Trough cross-stratified vf-m grained sandstone, common rippled reactivation surfaces, potential mud drapes and rip-up mud clasts, eventual desiccation cracks and/or evaporite-rich horizons. Thickness ranging between dm- to m values.	VF - M	Tidally-influenced migrating 3D-dunes.	Entrada Fm. Curtis Fm. Summerville Fm.
D	Structureless fluidised sandstone	Deformed to structureless fluidised of green to pink silt- to fine-grained sandstone, local fluid-escape and loading structures still visible, sometimes visually expressed as well rounded sandstone boulders with injected mudstone, maximum boulder Ø 25 cm, maximum bed thickness 2 m.	Si-F	Destruction of original sedimentary structures due to fluids flowing through the sandstone bed or through liquefaction of water-saturated horizons.	Entrada Ss Curtis Fm.
E	Thoroughly bioturbated condensed sandstone	Rusty-red condensed, cemented, fine-grained sandstone, thoroughly bioturbated., maximum thickness 25 cm.	F	Sediment starvation in a semi-arid coastal plane setting.	Entrada Ss
F	Matrix-supported basal conglomerate	Rounded to well-rounded, matrix-supported basal conglomerate, no preferred clast orientation but their long axis tend to be parallel to the bedding plane, matrix consists of f- to m-grained sandstone, maximum clast Ø 8 cm, maximum bed thickness 20 cm.	F-Pb	Flash flood deposits.	Curtis Fm. ?
G	Planar- to low angle cross- stratified sandstone	Plane-parallel- to low angle cross-stratified vf-f grained gray to green to white sandstone, potential herringbone cross-lamination, unidirectional current-, and oscillation ripple-lamination, as well as dm-scale soft sediment deformation, maximum individual bed thickness 60 cm.	VF - F	Upper shoreface to beach deposits with tidal influence.	Curtis Fm.
H	Tangential cross-stratified gravelly sandstone	Matrix-supported conglomeratic dune, hm-scale lateral extent, sub-horizontal erosive base, rip-up mud clasts, extra-basinal sub- to rounded clasts, maximum clast Ø 2.5 cm, unidirectional-current trough cross-stratification, maximum individual dune thickness 2.50 m.	M - Gr	High energy, asymmetric tidal flow pattern within a laterally restricted embayment.	Curtis Fm.
I	Tidally-influenced cross-stratified conglomeratic sandstone	Matrix- to clast-supported lense-shaped intraformational conglomerate of restricted lateral extent, locally developed and amalgamated in tidal bundles, rip-up mud clasts, extra-basinal sub- to rounded clasts, maximum clast Ø 2.5 cm, bidirectional cross-stratification with superimposed current-ripples, maximum bed thickness 60 cm.	F - Gr	High energy tidal channels-inlets.	Curtis Fm.
J	Planar to sigmoidal cross-stratified sandy conglomerate	Clast- to matrix-supported conglomerate, hm-scale lateral extent, convex-down erosive base, flat top, extra-basinal sub- to rounded clasts, maximum clast Ø 2.5 cm, planar cross-stratification, maximum individual thickness 3.00 m.	M - Gr	Point bar lateral accretion within a migrating tidal channel.	Curtis Fm.
K	Plane parallel-laminated mud- to siltstone	Plane parallel-laminated mud- to siltstone, scattered bidirectional current ripple cross-stratifications gray to green, occasional desiccation cracks, sporadic bioturbations both parallel and normal to the bedding planes.	Si - Cl	Gentle flow activity with tidally-related current reversals.	Curtis Fm.
L	Heterolithic silt- and sandstone with lenticular bedding	Rippled vf-f grained sandstone, grayish lenses containing herringbone and current ripple cross-stratifications within a matrix of laminated gray to green mud- to siltstones, occasional desiccation cracks, sporadic bioturbations both parallel and normal to the bedding planes.	Si - F	Current reversals in lower subtidal zone.	Curtis Fm.
M	Heterolithic silt- and sandstone with wavy bedding	Ripple cross-stratified vf-f grained grayish sand layers, with bi-directional current indicators and interbedded with laminated gray to green siltstone, occasional desiccation cracks, sporadic bioturbations both parallel and normal to the bedding planes, varying amount of organic matter.	Si - F	Current reversals in subtidal zone (shallower than Facies L).	Curtis Fm. Moab Mbr.
N	Heterolithic sandstone with flaser bedding	Ripple and herringbone cross-stratified vf-f gray to green to white sandstone, scattered mud lenses, as well as single and double mud drapes, varying amount of organic matter.	VF - F	Upper sub- to lower intertidal sandflat.	Curtis Fm.
O	Sandstone with climbing ripples	Climbing ripple cross-stratified vf-f grained sandstone, gray to green.	VF - F	Tidal channel overbank spill on tidal flat, Upper sub- to lower intertidal sandflat.	Curtis Fm.
P	Cross-stratified sandstone arranged in well-defined rhythmic tidal bundles	Vf-f(-m) grained gray to green to white sandstone, arranged in tidal bundles, with occasional anti-ripples documented from their toesets, varying amount of organic matter.	VF - F (-M)	Tidal inlets, lower energy than Facies I.	Curtis Fm.
Q	Structureless sandstone	Vf-f grained gray to green to white sandstone, massive, with potential scattered single and-or double mud drapes. Usually rounded and smoothly weathered.	VF - F	The nature of the lack of structure might only be due to intensive surface weathering. Presence of mud drapes indicate sub- or intertidal environment.	Curtis Fm.
R	Thoroughly bi-directional rippled cross-stratified sandstone	Thoroughly rippled silt- to vf-grained sandstone, dominated by herringbone cross-stratifications, potential climbing ripples.	S - VF	Deep subtidal environment with near equal flood and ebb tidal current conditions. Note that the weathering can in some cases erase most of the sedimentary structures.	Curtis Fm. Moab Mbr.
S	Plane parallel-stratified sandstone	Plane parallel-stratified vf-f-grained sandstone with scattered current ripple lamination, white, pink or green. Note that the weathering expression of this facies varies between the different units of the Curtis Fm. Potential mud cracks and soft sediment deformations.	(S -) VF - F	Tidal sandflat, upper flow regime (to lower antidune-regime?). Documented mud cracks indicate short-lived subaerial exposure.	Curtis Fm. Moab Mbr.
T	Condensed sandstone	Thin, yellow structureless sandstone, occasionally displaying low-amplitude undulations, exclusively observed capping the Moab Tongue Member of the Curtis Fm. Maximum bed thickness 10 cm.	(VF-F -) F	Condensed horizon.	Moab Mbr.
U	Rippled cross-stratified sandstone	Undulated to rippled cross-stratified vf-f-grained, gray to brown sandstone, with 3D current ripples, possible interference ripples, potential mud cracks and soft sediment deformations.	VF - F	3D migrating ripples under unidirectional current conditions.	Entrada Ss Curtis Fm. Moab Mbr. Summerville Fm.
V	Plane parallel-laminated siltstone	Dark red soft slope forming siltstone, most probably plane parallel-laminated, scattered pale white bleached lenses and evaporites.	Si	Supratidal plain.	Summerville Fm.
W	Iron rich ripple- and parallel-laminated sandstone	Dark red to brown cemented vf-f-grained sandstone, gentle ripple cross-stratifications, potential desiccation cracks.	VF - F	Fluvial overbank deposits.	Summerville Fm.
X	Palaeosol	Dark purple mud or silt.	M-S	sub-aerially exposed surface with superficial soil development.	Entrada Ss, Curtis Fm. Moab Mbr. Summerville Fm.

TABLE 2 - FACIES ASSOCIATIONS FOR THE ENTRADA SANDSTONE, CURTIS FORMATION AND SUMMERVILLE FORMATION

Facies Association	Depositional Environment	Facies Included	Formation
FA 1a	Coastal wet aeolian dune system (Kocurek and Havholm, 1993; Mountney, 2012), with episodic (marine) partial flooding of interdunes deposits and superficial development of soil- and vegetated horizons.	A, C, X	Entrada Sandstone Slick Rock Mbr.
FA 1b	Coastal wet aeolian interdune and lower coastal plain system (Kocurek and Havholm, 1993; Mountney, 2012), with episodic (marine) partial flooding of interdunes deposits and superficial development of soil- and vegetated horizons.	B, C, D, X	Entrada Sandstone earthy facies
FA 2	Beach deposits to upper shoreface deposits, with potential associated tidal channels cut-and-fill.	C, G, S, U	Curtis Fm.
FA 3a	Subtidal heterolithic mud-, silt- vf-grained sandstone, generally upward coarsening from laminated mudstone to wavy beddied sandstone, scarsely bioturbated.	H, I, J, K, L, M	Curtis Fm.
FA 3b	Subtidal heterolithic vf- to f-grained sandstone generally upward coarsening from wavy- to flaser bedded sandstone, scarsely bioturbated.	H, I, M, N	Curtis Fm.
FA 4a	Sandy tidal flat with correlative major tidal channels, with potential subaerial exposures.	S, U, X	Curtis Fm.
FA 4b	Tidal channel infills and splays, distal correlative of FA 4a in the northern areas.	C, H, I, L, M, N, S, U	Curtis Fm.
FA 5	High energy, sub- to intertidal sand -dominated environments, encompassing tidal flats, tidal channels, tidal dunes and tidal bars.	C, G, (K, L, M,) N, O, P, Q, R, S(, X)	Curtis Fm.
FA 6	Upper intertidal heterolithic channels and flats complex, upward finning, with intermittent prolonged subaerial exposures and rare bioturbation, indicator of a more stressed environment than FA 3.	K, L, M, N, Q, S, U, X	Curtis Fm.
FA 7	Coastal dry aeolian dune field (Mountney, 2012), arranged in five sequences separated by supersurfaces, upon which transgressive water-carried sediments and/or palaeosol can be observed.	A, N, Q, S, T, U, X	Curtis Fm. Moab Mbr.
FA 8	Supratidal lower coastal plain, with episodic marine flooding.	U, V, W, X	Summerville Fm.